

Aquaplanet Experiments Using CAM's Variable Resolution

Dynamical Core

COLIN M. ZARZYCKI, *

Department of Atmospheric, Oceanic, and Space Sciences, University of Michigan, Ann Arbor, Michigan, USA

MICHAEL N. LEVY

National Center for Atmospheric Research

CHRISTIANE JABLONOWSKI

University of Michigan

JAMES R. OVERFELT AND MARK A. TAYLOR

Sandia National Laboratories

PAUL A. ULLRICH

University of California, Davis

* *Corresponding author address:* Colin M. Zarzycki, University of Michigan, Department of Atmospheric, Oceanic, and Space Sciences, 2455 Hayward St., Ann Arbor, MI, 48109, USA.

E-mail: zarzycki@umich.edu

ABSTRACT

A variable-resolution option has been added within the Spectral Element (SE) dynamical core of the Department of Energy (DOE)-NCAR Community Atmosphere Model (CAM). CAM-SE allows for static refinement via conforming quadrilateral meshes on the cubed sphere. This paper investigates the effect of mesh refinement in a coupled climate model by running variable-resolution (var-res) simulations on an aquaplanet. The variable-resolution grid is a 2° (~ 222 km) grid with a refined patch of 0.25° (~ 28 km) resolution centered at the equator. Climatology statistics from these simulations are compared to globally-uniform runs of 2° and 0.25° .

A significant resolution dependence exists when using the CAM version 4 (CAM4) sub-grid physical parameterization package across scales. Global cloud fraction decreases and equatorial precipitation increases with finer horizontal resolution, resulting in drastically different climates between the uniform grid runs and a physics-induced grid imprinting in the var-res simulation. Using CAM version 5 (CAM5) physics significantly improves cloud scaling at different grid resolutions. Additional precipitation at the equator in the high-resolution mesh results in collocated zonally-anomalous divergence in both var-res simulations, although this feature is much weaker in CAM5 than CAM4. The equilibrium solution at each grid spacing within the var-res simulations captures the majority of the resolution signal of the corresponding globally-uniform grids. The var-res simulation exhibits good performance with respect to wave propagation, including equatorial regions where waves pass through grid transitions. In addition, the increased frequency of high-precipitation events in the refined 0.25° area within the var-res simulations matches that observed in the global 0.25° simulations.

1. Introduction

The past few decades have seen massive improvements in the performance of global atmospheric general circulation models. One important factor behind these gains is the decrease in horizontal grid spacing, allowing for direct resolution of features at smaller spatial scales. Better representation of processes such as precipitation, clouds, and turbulent transfer of heat, momentum, and moisture has contributed to quantifiable increases in model skill (Kalnay 2002; Lackmann 2011). The main restriction in achieving improved horizontal resolution is primarily the processing ability and memory constraints of the system used to run the model. As computational ability has improved, horizontal resolution has generally increased at a similar rate.

In some situations, modelers may be only concerned with a solution at a regional level. There are many reasons why this may be the case – making a local weather forecast, simulating regional climate, or comparing model output to observational statistics gathered locally. Traditionally, the use of limited area models (LAMs) (sometimes referred to as regional climate models) has allowed the achievement of these goals without expending extraneous computational resources in locations not critical to the scientific question at hand. Assuming computational burden is approximated by the number of grid cells tiling the domain, a LAM is an effective way of eliminating “wasted” resources used to calculate a solution which is not of interest to the modeler (ex: a scientist forecasting northern hemisphere tropical cyclones may not be immediately concerned with Antarctic dynamics).

Since LAMs are not global in nature, they require external forcing via lateral boundary conditions (LBCs) to drive the domain. Typically these LBCs are derived from a coarser, global model. In many cases, these driver models use different numerical formulations or physical parameterizations compared to the LAM. This may introduce non-physical biases into the child LAM (Laprise et al. 2008). In addition, there is question as to the well-posedness of prevalent flow-relaxation LBCs (McDonald 2003) and whether commonly used one-way nesting (the LAM “sees” the external boundary conditions but provides no feed-

back) properly allows for regional impacts of features requiring high-resolution (ex: tropical cyclones, mountain meteorology) to influence the global circulation.

Variable-resolution general circulation models (VRGCMs) may help serve to bridge the gap between global, uniform-grid GCMs and LAMs. These models are global in nature but generally use statically refined meshes to regionally increase resolution. A variable resolution mesh that is high resolution in a local region but significantly coarser over the rest of the globe has orders of magnitude fewer elements than a standard, global, high resolution mesh. This decreases the total number of degrees of freedom in the problem, reducing the wall clock time needed to complete the integration. However, since the model remains global in scope, it eliminates the need for externally-forced boundary conditions. It also unifies the global background circulation and the solution within the high-resolution nest and, since the same dynamical core and physics package can be used for all grid cells, minimizes the bias introduced by a different “driver” model.

Aside from studying regional weather or climate, VRGCMs can also be used as a key validation tool in assessing the resolution scalability of sub-grid physical parameterizations in globally-uniform simulations. Long-term climate simulations with a globally-uniform grid are typically expensive and, even with recent improvements in computer performance, generally require large blocks of wallclock time on massively parallel systems. As model resolution is increased, a thorough analysis is required to determine if the existing subgrid parameterizations perform adequately at the new horizontal grid spacings. Poorly-defined or poorly-tuned physical parameterizations can lead to a degradation of skill score and an unphysical climate. VRGCMs allow for multiple grid spacings within a single model run, meaning a suite of simulations at different resolutions used for tuning can be replaced by cheaper, single simulations. These simulations can help isolate performance changes in parameterizations that manifest themselves as changes in climate statistics with resolution and easily help researchers target specific facets of a model as areas for improvement.

A perhaps unintended side effect of introducing local refinement to global models has

been a discussion on how to properly evaluate a model with non-uniform meshes. St-Cyr et al. (2008) and Ringler et al. (2011) both show that small patches of refinement improve a solution locally but have minimal effect on the global error. Ringler et al. (2011) also note that convergence studies should be based on the resolution in the coarsest region because the global error from these regions will dominate the solution. Guba et al. (in prep.) ran several idealized shallow water test cases from Williamson et al. (1992) on variable-resolution, spectral element meshes with the same conclusions as found in St-Cyr et al. (2008) and Ringler et al. (2011). Therefore, we choose here to focus on qualitative results of introducing variable-resolution into coupled aquaplanet simulations.

In this paper we have two primary goals. One, we aim to evaluate the performance of mesh refinement in the Spectral Element option of the Community Atmosphere Model (CAM-SE) by comparing the climatology in a variable-resolution simulation with globally-uniform model runs. Two, we discuss the scale incognizance of both the CAM4 (Neale et al. 2010a) and CAM5 (Neale et al. 2010b) physics packages using prescribed default tunings. CAM is the atmospheric component of the Community Earth System Model (CESM) that is under development by the National Center for Atmospheric Research (NCAR) and various U.S. Department of Energy laboratories.

The paper is structured as follows. In Section 2 we discuss the model setup, including special modifications required to run CAM-SE on refined grids. In Section 3 we present the results of aquaplanet simulations using the CAM4 physics package. In Section 4 we complete the same simulations using the CAM5 parameterization and discuss differences between the packages. We also evaluate the impact of transition regions and refined cells on equatorial waves and the frequency of precipitation rates in Section 5. A recent update to CAM allows us to investigate the potential differences between using a bulk aerosol model and the newer modal aerosol package in CAM5 simulations which is discussed in Section 6. An informal discussion of the cost savings is found in Section 7. Conclusions are presented in Section 8.

2. Experimental Design

a. CAM-SE

The Spectral Element (SE) dynamical core (Taylor et al. (1997), Taylor and Fournier (2010), Taylor (2011), Dennis et al. (2012)) is one of four dynamical core options available in the Community Atmosphere Model. It became the default option (superseding the finite volume core) in CAM version 5.3.

CAM-SE uses the spectral element method to discretize in the horizontal direction, a finite-difference approach in the vertical with a hybrid sigma-pressure coordinate, and a Runge-Kutta time discretization (Dennis et al. 2012). The spectral elements are based on the cubed-sphere geometry (Sadourny 1972; Rančić et al. 1996; Ronchi et al. 1996). Cubed-sphere grids provide for quasi-uniformity over the global domain, eliminating issues with traditional grids such as converging meridians in polar regions which typically require short time steps or polar filtering to maintain numerical stability. This setup has been rigorously tested using uniform meshes both in a shallow water model (Taylor et al. 1997) and the 3D primitive equations (Fournier et al. 2004; Taylor et al. 2007). The accuracy of the model can be controlled by selecting the polynomial degree of the basis functions on each element. The default polynomial degree in CAM-SE is selected to be three (cubic polynomials), leading to fourth-order spatial accuracy.

Since the spectral element is a highly localized numerical discretization and requires minimal communication between processors on massively parallel computer systems, it is an ideal choice for future, high-resolution climate simulations. Dennis et al. (2012) and Evans et al. (2013) have shown that CAM-SE outperforms other dynamical cores in CAM at all processor counts for 0.25° resolution and finer and also scales nearly linearly up to one element per processor. As parallel computers continue to grow in size, CAM-SE is an attractive choice for high-resolution runs.

Because CAM-SE solves the primitive equations locally on individual elements, it pos-

sesses the ability to run on non-uniform grids without significant modifications to the underlying numerical scheme. The only two restrictions to running CAM-SE on non-uniform grids are that elements must be quadrilateral, and the refinement must be conforming (meaning every edge is shared by exactly two elements). Any conforming tiling of the sphere with quadrilaterals that satisfies these two criteria is acceptable.

Variable-resolution meshes are generated in CUBIT¹, a geometry and mesh generation toolkit created at Sandia National Laboratories. The user selects a base resolution and subsequently refines over an arbitrary number of regions of arbitrary spatial extent. CUBIT’s default quadrilateral refinement is a so-called “2-refinement.” Elements in the refinement region are divided into four and those bordering the region into three (Anderson et al. 2009). This technique is shown in Figure 1, and can be layered in such a way that the ratio of the edge size of the coarsest region to that of the finest region is any power of two. This technique leaves the global structure of the grid intact while only generating a narrow region containing cells distorted by the refinement where resolution transitions. This type of refinement, where resolution is increased by decreasing the area of the cubed-sphere elements while holding the basis function order fixed, is typically referred to as *h*-refinement.

The grid is only refined in the horizontal direction; each vertical column retains the same number of levels regardless of horizontal cell size. The numerical grid is read from an external file and generated during initialization. It remains fixed for the remainder of the simulation. The time step used in the dynamical core is restricted by a grid’s finest scale in order to satisfy the Courant-Friedrichs-Lewy stability (CFL) condition. Therefore, a globally-uniform 1° simulation will have the same dynamical time step as a 4° simulation with an area of refinement of 1°. For all cases (variable-resolution and uniform), the time step in a given run is identical for all grid cells regardless of resolution. While this means that coarse sections of variable-resolution grids are operating at shorter time steps than the CFL criteria requires, they generally constitute a small fraction of the total number of cells in a

¹<https://cubit.sandia.gov/>

variable-resolution simulation (the majority making up the high-resolution area of interest).

Unlike the time step, the coefficients for the explicitly-added horizontal diffusion (fourth-order hyperviscosity) are varied with gridscale within individual runs. The diffusion coefficient K_4 for an individual element can be calculated as

$$K_4(\Delta x) = K_4(\Delta x_{ref}) \left(\frac{\Delta x}{\Delta x_{ref}} \right)^y \quad (1)$$

where K_4 depends on the length of the longest axis of the element (Δx) and Δx_{ref} and $K_4(\Delta x_{ref})$ are a predetermined reference length and reference hyperviscosity coefficient to scale to.

The scaling power y is equal to 3.22, based on previously published tuning results for global spectral models (Boville 1991; Takahashi et al. 2006). Therefore, $K_4(\Delta x)$ decreases by approximately an order of magnitude for every halving of grid spacing. This scaling is selected so that the hyperviscosity coefficient in each region matches the operational default CAM-SE hyperviscosity for the uniform grid of that resolution.

b. Aquaplanet Experiment

The Aquaplanet Experiment² (APE), and, more specifically, the setup outlined as the “control” run in Neale and Hoskins (2000), is a simplified test for atmospheric models. The model setup consists of an ocean-covered Earth, therefore eliminating the effect of non-uniform topography on atmospheric flow. Surface forcing comes from prescribed zonally and hemispherically-averaged, sea surface temperatures that lie above the freezing level. There are no seasons and no planetary tilt, and the orbit has zero eccentricity, resulting in the model being in a state of constant equinox. Therefore, outside of the diurnal cycle in solar insolation there is no temporal change in forcing to the climate system.

These simplifications allow for an intermediate test which is more complex than dry dy-

²<http://www.met.reading.ac.uk/~mike/APE/>

namical core experiments, but simpler than full-climate simulations which may be coupled to active land, ocean, and ice models. Even with this simplified state, aquaplanet experiments have been shown to produce realistic climate features such as transient high and low pressure systems, convectively coupled equatorial waves, and tropical cyclones.

This is an interesting experiment to run with mesh refinement because there is no ‘solution’ to verify against. However, since the experiment uses identical, steady-state, zonally-uniform forcing conditions; we can isolate the effects of resolution without worrying about the contribution from other model components or feedbacks. Further, the use of zonally-averaged forcing allows us to isolate zonal asymmetries which may arise from inhomogenous refinement.

Using aquaplanet experiments to test CAM is not a novel concept. Both Williamson (2008a) and Li et al. (2011) showed that precipitation extremes in aquaplanet simulations using the CAM Eulerian spectral transform dynamical core and CAM3 physics parameterization did not converge with increasing resolution and fixed physics time step. A setup utilizing the Eulerian dynamical core and CAM4 physics (T42 resolution, approximately 2.8° grid spacing) was the NCAR’s contribution to the APE model intercomparison (Blackburn et al. 2013). Mishra et al. (2011) used CAM4 physics and an aquaplanet to test the rainfall characteristics within the HOMME (predecessor to SE) dynamical core. Rauscher et al. (2013) and Hagos et al. (2013) both used CAM4 physics to test the performance of the new Model Prediction Across Scales (MPAS, (Skamarock et al. 2012)) variable-resolution dynamical core. Aquaplanet climate simulations have also been used to investigate the representation of tropical cyclones at various resolutions in CAM (Li et al. 2013; Zarzycki et al. 2013).

c. Model grids

Three setups are used in this study. The details for these setups are outlined in Table 1. The main difference between the three is the mesh used – one run (referred to as “coarse”)

uses a uniform 2° (~ 222 km) grid, one (“fine”) uses a uniform 0.25° (~ 28 km) grid, and the final simulation (“var-res”) uses a grid that is 2° everywhere except for a roughly $90^\circ \times 90^\circ$ patch centered on the equator that is a 0.25° mesh (with a small transition region between the two). The $90^\circ \times 90^\circ$ patch is chosen so that the refinement is isolated to one face of the cubed-sphere grid. The coarse and var-res meshes are shown in Fig. 2. The coarse mesh contains 1,350 elements per model level, the fine grid has 86,400, and var-res has 10,609.

The simulations utilize the Community Atmosphere Model, version 5.1. All runs use one of two subgrid physical parameterizations packages which are options in CAM 5.1. The first set uses the CAM version 4 physics package (Neale et al. 2010a). There are 26 vertical levels and the physics routine is called every 600 seconds (10 minutes) for each simulation, regardless of horizontal resolution. The timestep is selected to match the CAM4 simulations in Williamson (2008b). This will be referred to as the CAM4 simulations. The second suite of simulations uses the CAM version 5 package (Neale et al. 2010b) with 30 levels and the physics called every 1800 seconds (30 minutes). These are the default physics time steps for each model setup at 1° (or equivalent) resolution. We have chosen to fix the physics time step because it has been shown that there is an implicit dependence of physics time step on model results (Williamson 2013). While Williamson (2013) showed that this dependence is smaller than the change in solution from using different horizontal grid spacing, varying the physics time step would result in another degree of freedom beyond the control state of the system.

The coarse simulations use a 600 second dynamical time step. The fine grid requires a smaller, 50 second dynamical time step to satisfy the CFL condition due to smaller horizontal grid spacing. The var-res simulations use the same 50 second dynamical time step since the model CFL condition is constrained by the highest resolution in the simulation.

All three simulations use different hyperviscosity coefficients, since, as discussed in Section 2a, hyperviscosity varies as a function of resolution. Where the var-res grid is identical to the coarse grid, the hyperviscosity values match, and the same is true with the fine grid. Other

than those specific differences, the parameterizations are identical across all three runs. All simulations use the default physics tunings at equivalent 1° resolution in CAM, although the differences in stock tuning parameters at other grid spacings are minimal.

The two uniform mesh simulations are run for 14 months, but the first two months are considered “spin-up.” Therefore, the analysis in the following sections only considers the final 12 months. The choice of two months of model spinup is supported by the findings of Williamson (2008a) who found that the model rapidly transitions to its own aquaplanet climate when starting from a closely related aquaplanet state (in our case, an equivalent spun-up APE state on a 1° uniform grid interpolated to the particular CAM-SE grid of interest).

The var-res simulations are run for 50 months, with results from the last 48 months analyzed. The additional run time was given to account for the fact that, near the equator, the fine region covered just 25% of the zonal band. However, preliminary results showed little difference in climate statistics between a 14 month run and a 50 month run, implying that the simulation rapidly adjusts to grid spacing, even in the variable-resolution case.

3. CAM4 Climatology

Two variables that have been commonly used to highlight differences between different resolutions in CAM aquaplanet simulations are cloud fraction and precipitation rate (Williamson 2008b). We therefore pay particular attention to vertically-integrated total cloud fraction (CLDTOT) and total precipitation rate (PRECT). Unless otherwise stated, all variables presented are climatological averages over the periods discussed at the end of Section 2c. Time averaging reduces variance in the results and, given the prescribed forcing, the APE climatology is zonally symmetric on a uniform mesh. Following the format of Williamson (2008a,b), we discuss global and zonal spatial averages of time-averaged data. Time-averaged contour plots are also included to highlight the effect of refinement.

The simulated global average total precipitation rates in CAM4 are 2.91 (coarse), 2.98 (var-res) and 3.09 (fine) mm day⁻¹. These values are in good agreement with the results of Mishra et al. (2011) who produced a time-averaged, global precipitation rate of 2.95 mm day⁻¹ in a 1° simulation using an earlier version of CAM-SE with CAM4 physics.

Due to the location of the refinement region, care had to be taken when determining where to average spatially to compare the var-res grid. Simple global averages disproportionately weight latitudes where the model resolution is coarse in all simulations. Figure 3 outlines the area of refinement and illustrates where the zonal / global averages were taken for the var-res grid. The low-resolution region of the var-res grid extends eastward from 60° E to 60° W, while the high-resolution region spans 30° W and 30° E. All averages (including the ones on the uniform grids) are taken between 25° S and 25° N so that the mid- and high-latitudes (where there is no high resolution in any of the simulations) do not affect the statistics. All spatial averages are area-weighted, despite being discussed in terms of latitude-longitude boxes.

There are two components to total precipitation in CAM; large-scale (resolved, or sometimes referred to as “stable”) precipitation and unresolved precipitation resulting from the subgrid convective parameterizations. Since large-scale precipitation is the resolved component of rainfall that is removed from the supersaturation of specific humidity in a gridbox, smaller grid spacing should improve the dynamical core’s ability to resolve convergent and vertical motions responsible for the production of precipitation. Therefore, if total precipitation (large-scale plus convective) is to remain scale-independent in climate models, there should be roughly a 1:1 tradeoff between any increase in large-scale precipitation and decrease in convective precipitation as resolution is increased. This trend should theoretically continue until all precipitation is fully resolved in the model, although the ability to run climate models at cloud-resolving (or finer) scales is still many years away. We will further discuss this scaling later.

Table 2 shows select area-weighted, time-averaged climate statistics in the equatorial band

($\pm 25^\circ$ N/S) for the three CAM4-SE simulations. Convective precipitation rates (PRECC) decrease as resolution is increased, whereas large-scale precipitation rates (PRECL) increase. The absolute increase in large-scale precipitation rates outweighs the decrease in convective rainfall, which can be easily verified by the increased total precipitation rate (PRECT, sum of PRECC and PRECL). The total precipitation rate in the low-resolution section of the var-res grid is higher than the corresponding uniform coarse grid. Conversely, it is higher in the fine grid than the matching, high-resolution section of the var-res mesh. These results imply that the precipitation does not respond to the grid immediately, but rather, the low-res grid influences the high-res component and vice versa.

The convective-to-large-scale precipitation ratio (C/L ratio) decreases with resolution (indicating higher resolution requires less adjustment from the convective scheme due to increased resolved updrafts). The C/L ratio matches across the uniform grids and the corresponding var-res region. The cloud fraction (CLDTOT) is significantly larger in the coarse mesh and the low-resolution component of the var-res grid than in either the fine grid or the refined section of the var-res mesh. Cloud fraction shows a well matched result in the coarse resolutions, but at 0.25° grid spacing, the var-res grid has a larger fraction than the fine grid. Since total cloud decreases significantly as resolution is increased in these simulations, this again implies the coarse component of the var-res grid is likely affecting the high-resolution patch. Total precipitable water (TPW) is approximately $1\text{-}1.5 \text{ kg m}^{-2}$ higher in the coarse simulations when compared to the fine grid scale.

Zonal averages for cloud fraction and total precipitation for CAM4-SE are shown in Fig. 4. Figure 4a compares the cloud fraction in the var-res simulation to the two uniform runs globally. These results can be compared to other models in the APE in Blackburn et al. (2013) (their Fig. 12). The solution in the coarse region of the var-res mesh (green) (beyond 30° latitude) produces very similar results to the solution of the coarse grid (blue). At all latitudes, cloud fraction decreases as resolution is increased (fine simulation, red), with the var-res simulation tending away from the coarse run and towards the fine in equatorial re-

gions, where roughly one-quarter of the equatorial band is simulated at high resolution. The monotonic decrease of cloud fraction as horizontal resolution is increased is a troublesome, but well-known issue with both the CAM3 and CAM4 physical parameterizations (e.g., Williamson (2008a,b), Rauscher et al. (2013), Hagos et al. (2013), O’Brien et al. (2013)).

Figure 4b only focuses on the band between 25° S and 25° N, and also divides the var-res model into its longitudinally-coarse region (60° E to 60° W) and fine region (30° W to 30° E) as shown in Figure 3. Results corresponding to the coarse portion of the var-res mesh are virtually indistinguishable from those of the global coarse mesh. In contrast, the high-resolution section of the var-res grid did not match the fine grid simulation, but rather, produced slightly higher cloud fraction near the equator. This suggests that the results in the refined domain did not quite achieve the resolution of the fine-scale simulation, but remain influenced by the flow in the coarse domain.

Similarly, Figure 4c shows the zonally-averaged total precipitation rates for the global domain. There is much better agreement between the three resolutions in profile shape and intensity outside of the tropics. The fine simulation has a slightly lower and more poleward peak in the mid-latitude precipitation maximum, likely associated with a small shift in extratropical storm tracks. In the equatorial band, all three simulations show a single intertropical convergence zone (ITCZ) peak centered at 0° latitude.

This absolute maximum increases with resolution and, like the cloud fraction in the equatorial band, the var-res simulation falls between the two globally-uniform simulations since its zonal average in this band is a combination of the two grid spacings. Figure 4d is the same as 4b except for total precipitation. In this case, the coarse region of the variable resolution mesh has a slightly larger average than the global coarse mesh at the equator, but is again indistinguishable outside the band of approximately 5° S to 5° N. The fine region, is well-matched with the global high resolution run at the equator, but north of 5° N and south of 5° S the global high resolution mesh produces slightly more precipitation. However, these changes are negligible at the global scale and may just be a function of the actual gridbox

(discretization) locations at these latitudes.

To investigate the spatial dependence of localized refinement, we show temporally-averaged global contour plots. Figures 5 (cloud fraction) and 6 (total precipitation rate) show the simulation results for all three grids (panels a-c), in addition to the difference plots between the var-res simulation and each uniform grid counterpart (panels d-e). The weak imprinting at coarser grid spacings is a result of remapping the data from the native cubed-sphere grid to a standardized latitude-longitude grid for analysis purposes. Figures 5a and 5c highlight the global decrease in cloud fraction with increasing resolution as seen in Figure 4a. The fractional decrease is relatively uniform globally, although it does maximize in the polar regions where cloud fraction decreases by nearly 50% between the coarse and fine simulations.

The extreme gridscale dependence of cloud fraction is also highlighted in the difference panels in Figs. 5d and 5e. Severe anomalies are seen associated with the region of increased resolution, both when comparing the var-res grid to the coarse and fine simulations. In addition, there also appears to be downstream impacts of the high-resolution patch as evidenced by the “tails” at approximately 25° N/S which extend eastward from the eastern periphery of the nest. This implies that, though CAM uses column physics (no knowledge of neighboring atmospheric conditions), cloud fraction does not uniformly and instantaneously assume the properties of the high-resolution nest. At the center of the latitude band where the refinement exists (15° N/S), the temporally-averaged zonal flow is easterly, meaning that the majority of parcels enter the high-resolution nest from the eastern side and exits through the western boundary. However, space-time diagrams of outgoing longwave radiation (not shown) imply that these tails are associated with frontal structures which are dragged from west-to-east across the poleward side of the high-resolution patch. Parcels transiting between resolutions which are associated with these features seem to maintain “memory” about their grid spacing and require an adjustment period to acquire the physical characteristics of the new resolution upon passage through a transition area.

While the var-res contour plots exhibit an obvious signature resulting from the high-

resolution patch, there is no readily apparent grid imprinting in the transition region. The fact that both the zonally-averaged and time-averaged plots show no observable spikes or other artifacts indicates the dynamical core is numerically handling the transition region appropriately. Additionally, the resolution signatures’ existence shows that the var-res simulation captures the resolution signal from the globally-uniform simulations within a single model run. This is highlighted by the regions where cloud fraction matches between the var-res and uniform grids in Figs. 5d and 5e (white areas).

Figures 6a-c show less of a gridscale dependence when total precipitation rate is considered. All three simulations exhibit a strong equatorial peak which dominates the global average. The difference plots (Figs. 6d,e) show that differences poleward of approximately 10° N/S are minor, a result already implied by Fig. 4c. In the equatorial band, increased resolution displays a gridscale dependence, with the peak precipitation being directly proportional to the resolution of the grid. Unlike cloud fraction, precipitation appears to incur a more instantaneous adjustment to grid resolution, with positive anomalies in Fig. 6d associated with the increased patch of resolution spanning the entire nest end-to-end and negative anomalies spanning the entire coarse latitude band in Fig. 6e. This “rapid” adjustment may be because there is a much greater fraction of large-scale (resolved) precipitation (Table 2) in the high-resolution nest, meaning the underlying grid is the dominant driver in the bias induced by the refinement. This may be different than the cloud parameterization scheme bias which is a function of both grid spacing and the atmospheric state advected into the high-resolution region.

As first outlined in Gill (1980), zonally-asymmetric diabatic heating in equatorial regions may drive a large-scale background circulation associated with anomalous upper level divergence. In the var-res simulation, a Gill response manifests itself due to the increase in resolution; total precipitation in the high-resolution patch is increased which adds additional latent heating to the atmosphere. Variable-resolution simulations using CAM4 physics have previously been shown to suffer from this issue (Rauscher et al. 2013). Figure 7a shows the

zonal anomaly (deviation from the zonal mean) of the time-averaged, vertically-integrated diabatic heating. Because of the increased precipitation rate (Fig. 6d), condensational warming is more prevalent in the high-resolution nest. This leads to anomalous divergence, shown in color contours in Fig. 7b. The most significant divergence bias is on the eastern portion of the nest. This is where near-equatorial flow first encounters the high-resolution nest. Since zonally-averaged total precipitable water is higher in the coarse region (Table 2), this represents a rapid adjustment where moisture is quickly removed from the column by the physics routine. This release leads to additional vertical velocities, and enhanced upper-level divergence. The divergence triggers an anomalous circulation reflected in the 200 hPa eddy streamfunction (line contours, Fig. 7b). The anti-cyclonic (cyclonic) anomalies to the west (east) of the high-resolution patch are similar to the ones seen in Rauscher et al. (2013) (their Figure 14a), who first highlighted the phenomenon in refined CAM4 simulations.

4. CAM5 Climatology

Almost all published literature using aquaplanet setups in CAM have utilized the legacy CAM3 and/or CAM4 physics packages (ex: Williamson (2008a,b), Li et al. (2011), Rauscher et al. (2013), among others). Very few studies have tested the new CAM5 subgrid physical parameterization package in an aquaplanet setup. Two examples are Reed and Jablonowski (2011) and O’Brien et al. (2013). However, they focused on specific research questions (tropical cyclones, cloud scaling) as opposed to more broad, general, long-term statistics.

a. Differences between CAM4 and CAM5 physics

For discussion, it is useful to highlight a few of the key differences between the CAM4 and CAM5 physics packages. The default number of vertical levels in CAM5 is 30 (compared to 26 in CAM4). The four additional levels in CAM5 are added below 700 hPa, increasing the total number of levels below 700 hPa from 5 to 9. This resolution in the lower troposphere was

added concurrently with a new planetary boundary layer and moist turbulence scheme based on diagnosed turbulent kinetic energy (Bretherton and Park 2009). This replaced the dry turbulence scheme of Holtslag and Boville (1993) based on specified K profiles. The surface flux parameterizations and deep convective scheme (Zhang and McFarlane 1995) remain the same between the two configurations. CAM4 uses a shallow convective parameterization outlined in Hack (1994) while CAM5 uses a newer scheme developed at the University of Washington (UW) (Park and Bretherton 2009). Another significant change in CAM5 is the use of prognostic double moment microphysics (Morrison and Gettelman 2008) with ice supersaturation (Gettelman et al. 2010). This is compared to prognostic single-moment microphysics (Rasch and Kristjánsson 1998) in CAM4. A more comprehensive discussion of these and other differences between CAM4 and CAM5 physics can be found in Neale et al. (2010b).

b. CAM5 Bulk Aerosol Model

We first run the CAM5 physics package with the prescribed aerosols within the Bulk Aerosol Model (BAM). This is the same model for aerosols used in the CAM4 simulations. The climatological dataset of aerosol mass concentrations is zonally, hemispherically, and temporally averaged to provide constant aerosol forcing which is symmetric about the equator and spatially distributed at latitudes similar to that seen in observations. This is the same setup used in Reed and Jablonowski (2011) and O’Brien et al. (2013).

Unlike CAM4, the updated CAM5 microphysics requires information about aerosols in specific modes (Morrison and Gettelman 2008). Since the prescribed BAM does not provide that information, an internal conversion in the physics package is required to allow for mass quantities to be treated in a modal sense for each gridbox. The aerosol mass mixing ratio is first multiplied by air density to produce a mass density. This mass density is multiplied by a number-to-mass conversion and a bulk scaling factor to arrive at the number of aerosols per volume. The parameterization of Abdul-Razzak and Ghan (2000) is then used to estimate

the number of activated aerosols by assuming an internal mixture within each of multiple aerosol modes. The cloud condensation nuclei count is then passed to the relevant routines.

c. CAM5 results

The globally-averaged CAM5 precipitation rates are 3.15 (coarse), 3.14 (var-res) and 3.12 (fine) mm day⁻¹. These quantities represent 8%, 5%, and 1% increases over the globally-averaged CAM4 simulations, respectively. Cloud fraction also increases. All global values fall within the range of models discussed in Blackburn et al. (2013) (their Figs. 10 and 11).

Equatorial band averages for simulations using the CAM5 physics packages can be seen in Table 3. The convective parameterization is significantly more active in CAM5, with higher PRECC totals at all resolutions compared to CAM4. This increase outweighs the corresponding decrease in large-scale precipitation, resulting in increased total precipitation rates.

Zonal averages of cloud fraction and total precipitation are plotted in Fig. 8. As shown in Fig. 8a, zonally-averaged cloud fraction is higher at all latitudes when compared to the CAM4 simulations (Fig. 4a). The distribution of cloud fraction is much less sensitive to changes in global resolution with all three distributions much closer to one another. The most dominant difference between the coarse and fine simulations is in polar regions, where there is a 5 to 10 percent decrease in cloud fraction as resolution is increased from 2° to 0.25°. In the CAM4 simulations, there is a change in the latitudinal gradient of cloud fraction poleward of approximately 60° N/S (cloud fraction increases with latitude in the coarse simulation, decreases with latitude in the fine simulation, Fig. 4a). This reversal still occurs in the CAM5 simulation, but is much weaker. Figure 8b highlights the component resolutions of the equatorial band. Peak cloud fraction near the equator are essentially identical, regardless of resolution. There are small differences in the subtropics between resolution, but these differences are significantly smaller than seen in Fig. 4b (CAM4).

The equatorial peak of precipitation rates (Figs. 8c and 8d) in the fine grid are approx-

imately 17% less in CAM5 (25 mm day^{-1}) when compared to CAM4 (30 mm day^{-1}). The peak in the coarse simulation drops similarly, falling from 23 mm day^{-1} (CAM4) to 18 mm day^{-1} (CAM5). Figure 8d (CAM5) shows similar results to Fig. 4d (CAM4) in that the fine (coarse) simulation and the high resolution (low resolution) component of the var-res grid are quite similar. This indicates that the dynamical behavior at each grid scale in the var-res simulation is similar to the corresponding uniform run.

Temporally and spatially-averaged contour plots are shown in Figs. 9 and 10. For cloud fraction in the CAM5 simulation, the plots (Figure 9d-e) of the difference between the var-res grid and the corresponding uniform simulations do not show obvious grid imprinting resulting from the resolution-dependence of the parameterizations which control cloud fraction as they did with the CAM4 package (Figs. 5d-e). In addition to the significant decrease in scale sensitivity, the asymmetric downstream effects seen in the CAM4 simulations do not appear in the CAM5 runs.

The spatial precipitation analysis (Fig. 10) shows that, unlike cloud fraction, the scale-dependent nature of the total precipitation rate is not significantly altered by using CAM5 physics. Like the CAM4 simulations (Fig. 6), the var-res simulation shows a positive zonal precipitation anomaly in the refined region when compared to the coarse grid (Fig. 10d). The opposite is true (outside the refinement patch) when comparing the same run to the fine simulation (Figure 10e). The overall difference between the resolutions is slightly smaller in total magnitude, although this may be a result of the fact that the CAM5 APE simulations produces less total precipitation right at the equator (where the largest anomalies occur) than the CAM4 simulations.

Interestingly, small bands of positive anomalies appears in Fig. 10e that surround the negative differences at the equator. While total precipitation increases at the equator with increasing resolution in CAM5, some of this increase is balanced by a narrowing of the precipitation peak (also seen in Fig. 8d). To verify this is not a function of the output resolution being higher for the fine simulations, all output was remapped to the coarse grid and the

same result was observed (not shown). This narrowing may be due to an increase in Hadley cell strength with resolution. This has been shown to occur in CAM and leads to enhanced vertical velocities at the equator (Rauscher et al. 2013). This therefore results in increases in large-scale precipitation, since it is sensitive to resolved motion in the atmosphere. This narrowing is also the reason why more area-weighted total precipitation is simulated with the coarse grid in the equatorial band spanning 25° N/S, as listed in Table 3 (PRECT). Even though the ITCZ maximum increases with resolution, the shape of the peak is sufficiently compressed to allow the loss of spatial coverage to offset the increased maximum. Blackburn et al. (2013) also noted that compensating effects of maximum precipitation and spatial width of the ITCZ moderated tropical precipitation variance in a multi-model APE survey. The fact that integrated tropical precipitation (as in Table 3) is similar at multiple resolutions even with different equatorial maxima could be a manifestation of this feedback.

As seen in Fig. 11, the Gill-type response elicited by the high-resolution nest is still evident, but damped, when using the CAM5 physics package. A band of zonally anomalous vertically-integrated heat release can be seen in the high-resolution patch of the var-res grid in Fig. 11a. This is associated with the additional total precipitation induced by the increase in resolution which is shown in Fig. 10. This band is slightly wider, but approximately half as strong as in Fig. 7a (CAM4).

Interestingly, the maximum heating occurs on the western edge of the nest (where equatorial flow is preparing to exit the high resolution region). This result is opposite to that seen in the CAM4 simulations, which had a single, strong peak in anomalous diabatic heating on the eastern (entry) edge of the nest. Since dynamical core attributes such as the grid, time step, and diffusion are all identical for the CAM4 and CAM5 simulations, it suggests that this response is a function of the physics package.

Figure 11b shows that the anomalous 200 hPa divergence associated with the high-resolution nest is significantly reduced. While there still is anomalous rotational flow at 200 hPa as evidenced by the eddy streamfunction contours, the pattern which matches that seen

in Gill (1980) and Rauscher et al. (2013) is not as evident as in Fig. 7b (CAM4). While a scale-dependent aspect of total precipitation is still evident in the aquaplanet simulations, the use of CAM5 physics appears to mitigate VRGCM-induced thermal circulations.

5. High-frequency wave analysis

In addition to the climatological averages, 6-hourly output from the CAM5 simulations was used to analyze wave features and precipitation extremes produced. The main point of interest is whether these were significantly affected by the variable resolution, and in particular, the transition regions. Since the model physics are column-based, we do not expect the results to differ much if this study was undertaken for the CAM4 physics. Our CAM4 simulations did not produce output at a high enough temporal frequency for the following analyses.

1) EQUATORIAL WAVE ACTIVITY

Wavenumber-frequency diagrams, following the spectral analysis methodology of Wheeler and Kiladis (1999) are shown in Fig. 12. Following Williamson (2008a) and Blackburn et al. (2013), we plot the full power without normalizing by the background spectrum. Normalization is typically performed because it helps isolate spectral peaks with specific modes. However, it also removes the resolution dependence contained in the background spectrum. Figures 12a and 12c show this unnormalized symmetric component of the spectra of 6-hour outgoing longwave radiation (OLR) for the coarse (2°) and fine (0.25°) grids, respectively. As resolution is increased, total power in high-frequency eastward waves decreases, while the opposite is true for high-frequency westward waves. Figures 12d and 12f are the same for the anti-symmetric component. The variable-resolution results are shown in Figure 12b (anti-symmetric) and Figure 12e (symmetric).

In both cases, variable-resolution does not significantly alter the solution. There are no

obvious peaks that can be attributed to spurious wave interaction with resolution changes resulting in parasitic modes. The results are very similar to both the fine and coarse region, and, in many cases, appear to represent a “transition” between the two simulations. An example of this would be the decrease in high-frequency (greater than 0.35 cycles per day) Kelvin-type waves (symmetric panels, Figure 12d-f). The power decreases in this spectral region from the coarse to the var-res simulation and then the var-res to the fine simulation. The exact reasoning behind this difference is unclear. Given the fact that parameterized convective activity is higher in the coarse runs (see Table 3), this may be a high-frequency signal heavily influenced by the convective scheme operating on near-diurnal scales, or it may be a result of “noise” induced by small-scale structure in the high-resolution simulations.

Figure 13 shows one-year Hovmöller diagrams of OLR for each of the grid types in the CAM5 simulations. OLR is averaged between 10° N/S. In the var-res grid (Fig. 13b), the longitudes of the transition regions are demarcated using black vertical lines. The solid black contours are band-pass filtered values of OLR corresponding to Kelvin wave activity. There is a slight decrease in background OLR when resolution is increased from the coarse to the fine grid. This agrees with Figs. 4a-b which show less cloud fraction in the high-resolution simulation. The var-res grid reflects this with lower OLR values during non-Kelvin wave events in the high-resolution region.

In the var-res simulation, there is no significant change in slope or kinking of the contours, which would represent a change in the phase speed of the wave activity upon interaction with a transition region. This is similar to the findings in Zarzycki et al. (2013) where cyclonic vortices interacting with mesh transition regions in similar setups of CAM-SE did not exhibit artificial wave reflection or distortion.

2) PRECIPITATION FREQUENCY

Histograms of precipitation rate frequency in the three CAM5 simulations are shown in Fig. 14. Statistics are calculated in a band extending 10° N/S from the equator using 6-

hourly instantaneous total precipitation rate output. The variable-resolution analysis is split by grid spacing, using the boundaries shown in Fig. 3. Output is conservatively remapped to a uniform 2° grid based on the recommendations of Chen and Knutson (2008). Both Figs. 14a and 14b show the same data, with Fig. 14a only focusing on precipitation values less than 120 mm day^{-1} .

Even after remapping, both panels show an increase in the frequency of extreme events with higher resolution. The coarse grid and low-resolution component of the var-res grid both have a higher frequency of low precipitation events. For this model setup, the equilibrium point where the two simulations cross (are at equal frequencies) is approximately 32 mm day^{-1} . The histograms for the coarse and fine grids match their corresponding var-res resolution well. This is another indication that dynamically, the model behaves as expected in each regime. We note that the globally-uniform fine grid has a slightly longer tail than the high-resolution patch in the var-res run (Fig. 14b). There appears to be a small upscaling/downscaling effect where parcels at the edge of the sampling area (red hatch, Fig. 3) have not fully adapted to the high-resolution nest yet. This is confirmed by shrinking the area of analysis by 5° in the latitudinal direction, which shows better agreement for extreme events (not shown). This may have implications on the “buffer” area required for regional climate-type simulations as well as whether or not wider transition regions are needed to allow for the flow to adjust to the grid spacing. Given CAM-SE’s high-order numerics, dynamical features are resolved well, even with fairly abrupt transitions. However, the solution may be improved in coupled climate systems by broadening this transition given current column-based subgrid parameterizations.

6. CAM5 Modal Aerosols

While completing the previously discussed simulations, CAM version 5.3 was released, providing support for prescribed modal aerosols in the Modal Aerosol Model (MAM). The re-

lease provides a climatological dataset containing information about modeled aerosol species. This dataset is used as an input to the model with the active chemistry package turned off. This is similar to the bulk aerosol model discussed earlier, however, the model now supports variation in aerosol concentration within species-specific modes. In contrast, BAM with CAM5 provides only bulk mass concentrations for a specific species, which are empirically converted to modes within the model physics.

We follow the same steps discussed earlier to generate an aquaplanet-type aerosol distribution. The data set was first time-averaged to provide temporally-homogenous fields. In this case, each aerosol mode was averaged separately, allowing for latitudinal variation in ratio of modes (such as fine-to-coarse, etc.). Our model results so far indicate that solutions at particular grid spacings within variable-resolution simulations do a satisfactory job matching their uniform counterpart. Therefore, we have only completed var-res simulations.

Figure 15 displays the zonally-averaged cloud fraction and total precipitation for CAM5 coupled to both aerosol packages with the var-res configuration. Figures 15a and 15c show the global zonal averages for cloud and precipitation while Figs. 15b and 15d differentiate between the fine and coarse grid components in the equatorial band. Global cloud fraction is largely unchanged between the two aerosol packages. The largest difference exists in the ITCZ where MAM produces about 4% less cloud fraction than BAM. MAM appears to be slightly more scale-selective as shown in Fig. 15b. Like cloud fraction, precipitation is largely matched between the two simulations outside of the latitudes in the immediate vicinity of the equator. Simulations utilizing the MAM produce slightly less precipitation in both the fine and coarse components of the grid.

This result, while generally qualitative in nature, may have implications for climate studies using prescribed aerosols. Using prescribed aerosols greatly reduces the computing requirements for the CAM5 physics package and may allow users with limited resources to use the new CAM5 physics versus a less expensive, but older, set of subgrid parameterizations. While global quantities of cloud and precipitation are similar, differences are not insignificant

at the equator in these simplified simulations. This may translate to a bias in tropical clouds and precipitation in coupled runs using prescribed aerosols, although further work is necessary to confirm whether or not this is the case. In addition, the difference in simulation results from using the two different techniques for prescribing aerosols in CAM5 is smaller than the differences between various resolutions in CAM4. This also serves to confirm that the CAM5 physics does not suffer from as much scale sensitivity as CAM4, since it retains consistent results across scales, even with two different aerosol forcing packages.

7. Performance and Timing

Since the focus of this study is a comparison of the climate predicted by variable resolution meshes rather than collecting more formal timing results a detailed study was not performed. However, some meaningful data was collected. Here, we only discuss the CAM4 simulations. Since the CAM5 physical parameterization is also column-based, the scaling results for those runs should be essentially identical, and preliminary results (not shown) imply that this is the case.

All CAM4 simulations were run on the same computing hardware (Red Sky at Sandia National Laboratories), although not necessarily on the same nodes. Since the var-res simulation and the fine grid simulation use the same time step, the only variation in timing is expected to come from the number of elements in the mesh.

As mentioned in Section 2 and shown in Table 1, the uniform 0.25° grid contains approximately eight times more elements than the refined var-res setup, so it is expected to run about 8 times slower. The variable-resolution simulation achieved 3.84 simulated years per day (SYPD) on 400 cores, while the high-resolution simulation ran at 1.35 SYPD on 1,280 cores. Assuming linear scalability, that translates into 0.42 SYPD on 400 cores, more than 9 times slower than var-res.

For completeness, the coarse simulation ran at 42.5 SYPD on 160 cores, equivalent to 106

SYPD on 400 cores, which is just over 250 times faster than the fine run. This is expected because there is a factor of 64 fewer elements and the dynamics time step is 12 times larger. As mentioned earlier, the physics time step was held constant across all runs.

Since there was not significant effort to control these factors for a formal timing study, these results should be taken as an aside. The primary goal of our study is the analysis of the model statistics in coupled, aquaplanet simulations. Small deviations from perfect scaling are inevitable due to factors such as initialization cost, latency bottlenecks, input/output constraints and noise introduced by random node selection. However, the fact that model runtime was close to predicted values given linear scaling is promising.

8. Conclusions

The spectral element dynamical core in the Community Atmosphere Model supports mesh refinement based on quadrilateral, conforming grid elements. Using a refined mesh provides a method to collect high resolution climate statistics in a particular area of interest while producing a low resolution simulation outside the region, reducing the computational cost of running CAM. The effectiveness of variable resolution meshes in CAM-SE was shown by running the aquaplanet control test from Neale and Hoskins (2000) and analyzing the global and zonal averages of quantities such as total cloud fraction and precipitation. Both CAM4 and CAM5 physics were tested to investigate the scale-sensitivity of the physics parameterizations and test the dynamical core as an option for use in climate simulations. Model throughput was improved tremendously with variable-resolution due to the lower number of grid cells and, therefore, decreased computational cost. All simulations show that a high-resolution nest embedded within a coarse global grid generally matches climate statistics produced by a corresponding uniform high-resolution grid.

Variable-resolution simulations with CAM4 physics show a significant resolution signature in both integrated cloud fraction and total precipitation rate, with these signatures

focused in or near the region of refinement. The statistics in the refined patch match results from globally-uniform simulations with the same model, indicating these issues are a deficiency in the model physics not being scale-aware as opposed to an issue in the variable-resolution implementation in the CAM-SE dynamical core.

Simulated total cloud fraction in CAM5 is increased over CAM4. This increase occurs at all latitudes, and, while most pronounced at the poles, is not dominated regionally. Both cloud fractions fall well within the range of model performance in the Aquaplanet Experiment (Blackburn et al. 2013). Convection is significantly more active in CAM5 than CAM4, which is an interesting result since both versions of the model use the same convective scheme. One likely culprit is CAM5’s updated microphysics. Even though the convection routine is called first in the moist physics calling sequence, a less active microphysics scheme (in terms of large-scale precipitation removed from the atmosphere) leaves more water available to the convective scheme at subsequent time steps. Another possible cause might be that CAM5’s updated boundary layer scheme moistens the lower domain of the troposphere more effectively thus providing more favorable conditions for convection. Unfortunately, given the strong interdependency of physics packages in current climate models, it is extremely difficult to disentangle the individual impact one factor might have on a specific process in these simulations.

We note that recent work such as Williamson (2008a) and O’Brien et al. (2013) argue this may not be the correct way to approach resolution dependence in this framework. True convective precipitation generally occurs at less than 10 km grid scales, and therefore should remain relatively fixed. However, Reed and Jablonowski (2012) showed in simplified simulations at 55 and 28 km grid spacing that only a large-scale condensation routine was necessary to produce realistic precipitation in a convectively-dominated system (tropical cyclones). These results suggest that additional clarity is needed in denoting exactly how precipitation is partitioned at hydrostatic resolutions.

In addition, the overt grid scale dependence of total cloud fraction seen in CAM4 simula-

tions appears to be significantly improved with the CAM5 physics package. The fact that no visible grid imprinting is seen in Fig. 9c is a good indicator that physical parameterizations involved in cloud formation behave well in a variable-resolution framework. They adjust ‘rapidly’ to the underlying grid resolution within a single simulation without the need for variable tuning between the different sized elements. This improved cloud scaling is also observed in O’Brien et al. (2013), who postulate that this improvement is a function of the new Morrison-Gettleman microphysics package. This implies that the Rasch-Kristjansson microphysics scheme in CAM4 might significantly contribute to the resolution dependence in the CAM4 simulations.

An increase in precipitation with resolution is seen with both physics packages, although the magnitude of this sensitivity is higher for CAM4. Given the addition of a refined patch, this sensitivity excites a diabatic heating anomaly in the zonal direction. This heating forces an anomalous circulation which exists due to the high-resolution nest. The CAM4 simulations show an obvious response to the heating, similar to that seen in Rauscher et al. (2013). The diabatic heating anomaly, while still existent, is weaker in CAM5. This leads to less upper-level divergence and a weaker circulation response. However, it is unknown whether either anomaly would have a significant impact on climate statistics in a fully-coupled VRGCM simulation.

Interestingly, the peak zonally-anomalous divergence in the tropics in the CAM4 simulations occurs at the nest entrance (eastern edge) while this peak occurs near the nest exit (western edge) in CAM5. This implies that the moist physics/gridscale feedback is altered in CAM5. This may be due to the modified microphysics scheme. The Morrison-Gettleman microphysics (CAM5) may not respond as “harshly” to abrupt grid resolution changes which allow the equatorial flow in the ITCZ to more slowly adapt to the high-resolution nest. The CAM5 result (diabatic heating anomaly near nest exit) is actually more similar to the results seen in Rauscher et al. (2013), although they used CAM4 physics. Since their grid transition region is much more gradual, it also suggests a strong gridscale feedback is inherent in the

CAM4 physics.

Equatorial waves in the CAM5 simulations show that CAM-SE’s numerics perform well when atmospheric features transit through a resolution discontinuity into a high-resolution nest. No anomalous variance is seen in Wheeler-Kiladis diagrams. The variable-resolution qualitatively appears to bridge fine and coarse simulations. Temporal analysis also qualitatively shows that Kelvin wave features do not incur phase speed shifts upon entry and exit of the high-resolution patch. Additionally, individual precipitation events show similar frequency at specified grid spacings, further confirming that the flow in the high-resolution nest within the var-res grid behaves in the same fashion as a globally-uniform fine grid.

Computational cost is saved by reducing the number of elements in the grid. Dennis et al. (2012) and Evans et al. (2013) both show that CAM-SE scales nearly linearly, so reducing the number of elements also reduces the number of cores needed to maintain throughput. The decreased computational demands make it significantly faster to generate an ensemble of runs, which will greatly speed up the process of tuning the model or testing new physical parameterizations.

Future work will involve testing variable-resolution in CAM-SE in fully-coupled simulations. While the CAM5 physics package would appear to be a superior choice in variable-resolution simulations due to the improved cloud fraction scaling, other processes, such as precipitation, still exhibit a resolution signature. Previous work with the dry CAM-SE dynamical core (Zarzycki et al. 2013; Guba et al. in prep.) showed that any numerical errors arising from grid refinement are small. This suggests that the resolution signatures seen in this study are the result of the physics packages.

Further work may be necessary to modify existing parameterizations such that they behave in a more scale-independent manner. In addition, more widespread adaptation of variable-resolution models in weather forecasting or climate assessments may push for a paradigm shift in subgrid parameterization development, requiring novel fully scale-aware approaches for seamless prediction across scales.

Acknowledgments.

C.M.Z. and C.J. were supported by the Office of Science, U.S. Department of Energy (DOE), Award No. DE0003990 and DE-SC0006684. In addition, M.N.L., J.R.O., and M.A.T. were supported by the DOE Office of Biological and Environmental Research, work package 12-015334 and 06-13194. Parts of the research and computations were done at Sandia National Laboratories, a multi-program laboratory managed and operated by Sandia Corporation, a wholly owned subsidiary of Lockheed Martin Corporation, for DOE's National Nuclear Security Administration under contract DE-AC04-94AL85000. Additional computations were completed using the National Center for Atmospheric Research's (NCAR) computing resources as well as those at the University of California at Davis.

REFERENCES

- Abdul-Razzak, H. and S. J. Ghan, 2000: A parameterization of aerosol activation: 2. Multiple aerosol types. *Journal of Geophysical Research: Atmospheres*, **105 (D5)**, 6837–6844, doi:10.1029/1999JD901161.
- Anderson, B. D., S. E. Benzley, and S. J. Owen, 2009: Automatic all quadrilateral mesh adaption through refinement and coarsening. *Proceedings of the 18th International Meshing Roundtable*, B. W. Clark, Ed., Springer Berlin Heidelberg, 557–574, doi:10.1007/978-3-642-04319-2_32.
- Blackburn, M., et al., 2013: The Aqua-Planet Experiment (APE): Control SST simulation. *Journal of the Meteorological Society of Japan*, **91A**, 17–56, doi:10.2151/jmsj.2013-A02.
- Boville, B. A., 1991: Sensitivity of simulated climate to model resolution. *Journal of Climate*, **4 (5)**, 469–485.
- Bretherton, C. S. and S. Park, 2009: A new moist turbulence parameterization in the Community Atmosphere Model. *Journal of Climate*, **22 (12)**, 3422–3448, doi:10.1175/2008JCLI2556.1.
- Chen, C.-T. and T. Knutson, 2008: On the verification and comparison of extreme rainfall indices from climate models. *Journal of Climate*, **21 (7)**, 1605–1621, doi:10.1175/2007JCLI1494.1.
- Dennis, J. M., et al., 2012: CAM-SE: A scalable spectral element dynamical core for the Community Atmosphere Model. *International Journal of High Performance Computing Applications*, **26 (1)**, 74–89, doi:10.1177/1094342011428142.

- Evans, K. J., P. H. Lauritzen, S. K. Mishra, R. B. Neale, M. A. Taylor, and J. J. Tribbia, 2013: AMIP simulation with the CAM4 spectral element dynamical core. *Journal of Climate*, **26** (3), 689–709, doi:10.1175/JCLI-D-11-00448.1.
- Fournier, A., M. A. Taylor, and J. J. Tribbia, 2004: The spectral element atmospheric model: High-resolution parallel computation and response to regional forcing. *Mon. Wea. Rev.*, **132**, 726–748.
- Gettelman, A., et al., 2010: Global simulations of ice nucleation and ice supersaturation with an improved cloud scheme in the Community Atmosphere Model. *Journal of Geophysical Research: Atmospheres*, **115** (D18), doi:10.1029/2009JD013797.
- Gill, A. E., 1980: Some simple solutions for heat-induced tropical circulation. *Quarterly Journal of the Royal Meteorological Society*, **106** (449), 447–462, doi:10.1002/qj.49710644905.
- Guba, O., J. R. Overfelt, M. A. Taylor, M. N. Levy, and P. A. Ullrich, in prep.: The spectral element method on variable resolution grids: Evaluating grid sensitivity and resolution-aware numerical viscosity.
- Hack, J. J., 1994: Parameterization of moist convection in the National Center for Atmospheric Research Community Climate Model (CCM2). *J. Geophys. Res.*, **99**, 5551–5568, doi:10.1029/93JD03478.
- Hagos, S., R. Leung, S. A. Rauscher, and T. Ringler, 2013: Errors characteristics of two grid refinement approaches in aqua-planet simulations: MPAS-A and WRF. *Monthly Weather Review*, **141**, 3022–3036, doi:10.1175/MWR-D-12-00338.1.
- Holtslag, A. A. M. and B. A. Boville, 1993: Local versus nonlocal boundary-layer diffusion in a global climate model. *J. Climate*, **6**, 1825–1842.
- Kalnay, E., 2002: *Atmospheric Modeling, Data Assimilation, and Predictability*. Cambridge University Press, 364 pp.

- Lackmann, G., 2011: *Midlatitude synoptic meteorology: dynamics, analysis, and forecasting*. American Meteorological Society, Boston, Mass., 345 pp.
- Laprise, R., et al., 2008: Challenging some tenets of regional climate modelling. *Meteorology and Atmospheric Physics*, **100** (1-4), 3–22, doi:10.1007/s00703-008-0292-9.
- Li, F., W. D. Collins, M. F. Wehner, and L. R. Leung, 2013: Hurricanes in an aquaplanet world: Implications of the impacts of external forcing and model horizontal resolution. *Journal of Advances in Modeling Earth Systems*, **5** (2), 134–145, doi:10.1002/jame.20020.
- Li, F., W. D. Collins, M. F. Wehner, D. L. Williamson, J. G. Olson, and C. Algieri, 2011: Impact of horizontal resolution on simulation of precipitation extremes in an aqua-planet version of Community Atmospheric Model (CAM3). *Tellus Series A*, **63**, 884–892, doi:10.1111/j.1600-0870.2011.00544.x.
- McDonald, A., 2003: Transparent boundary conditions for the shallow-water equations: Testing in a nested environment. *Monthly Weather Review*, **131** (4), 698–705.
- Mishra, S. K., M. A. Taylor, R. D. Nair, P. H. Lauritzen, H. M. Tufo, and J. J. Tribbia, 2011: Evaluation of the HOMME dynamical core in the aquaplanet configuration of NCAR CAM4: Rainfall. *J. Climate*, **24**, 4037–4055, doi:10.1175/2011JCLI3860.1.
- Morrison, H. and A. Gettelman, 2008: A new two-moment bulk stratiform cloud microphysics scheme in the Community Atmosphere Model, version 3 (CAM3). part i: Description and numerical tests. *Journal of Climate*, **21** (15), 3642–3659, doi:10.1175/2008JCLI2105.1.
- Neale, R. B. and B. J. Hoskins, 2000: A standard test for AGCMs including their physical parametrizations: I: The proposal. *Atmospheric Science Letters*, **1** (2), 101–107.
- Neale, R. B., et al., 2010a: Description of the NCAR Community Atmosphere Model (CAM

- 4.0). NCAR Technical Note NCAR/TN-485+STR, National Center for Atmospheric Research, 212 pp., Boulder, Colorado.
- Neale, R. B., et al., 2010b: Description of the NCAR Community Atmosphere Model (CAM 5.0). NCAR Technical Note NCAR/TN-486+STR, National Center for Atmospheric Research, 268 pp., Boulder, Colorado.
- O'Brien, T. A., F. Li, W. D. Collins, S. A. Rauscher, T. D. Ringler, M. A. Taylor, S. M. Hagos, and R. L. Leung, 2013: Observed scaling in clouds and precipitation and scale incognizance in regional to global atmospheric models. *Journal of Climate*, **26**, 9313–9333, doi:10.1175/JCLI-D-13-00005.1.
- Park, S. and C. S. Bretherton, 2009: The University of Washington shallow convection and moist turbulence schemes and their impact on climate simulations with the Community Atmosphere Model. *Journal of Climate*, **22** (12), 3449–3469, doi:10.1175/2008JCLI2557.1.
- Rančić, M., R. J. Purser, and F. Mesinger, 1996: A global shallow-water model using an expanded spherical cube: Gnomonic versus conformal coordinates. *Quarterly Journal of the Royal Meteorological Society*, **122** (532), 959–982, doi:10.1002/qj.49712253209.
- Rasch, P. J. and J. E. Kristjánsson, 1998: A comparison of the CCM3 model climate using diagnosed and predicted condensate parameterizations. *Journal of Climate*, **11** (7), 1587–1614.
- Rauscher, S. A., T. D. Ringler, W. C. Skamarock, and A. A. Mirin, 2013: Exploring a global multiresolution modeling approach using aquaplanet simulations. *Journal of Climate*, **26** (8), 2432–2452, doi:10.1175/JCLI-D-12-00154.1.
- Reed, K. A. and C. Jablonowski, 2011: An analytic vortex initialization technique for idealized tropical cyclone studies in AGCMs. *Monthly Weather Review*, **139** (2), 689–710, doi:10.1175/2010MWR3488.1.

- Reed, K. A. and C. Jablonowski, 2012: Idealized tropical cyclone simulations of intermediate complexity: A test case for AGCMs. *Journal of Advances in Modeling Earth Systems*, **4**, M04001, doi:10.1029/2011MS000099.
- Ringler, T. D., D. Jacobsen, M. Gunzburger, L. Ju, M. Duda, and W. Skamarock, 2011: Exploring a multiresolution modeling approach within the shallow-water equations. *Monthly Weather Review*, **139** (11), 3348–3368, doi:10.1175/MWR-D-10-05049.1.
- Ronchi, C., R. Iacono, and P. Paolucci, 1996: The “cubed sphere”: A new method for the solution of partial differential equations in spherical geometry. *Journal of Computational Physics*, **124** (1), 93 – 114, doi:10.1006/jcph.1996.0047.
- Sadourny, R., 1972: Conservative finite-difference approximations of the primitive equations on quasi-uniform spherical grids. *Mon. Wea. Rev.*, **100**, 136–144.
- Skamarock, W. C., J. B. Klemp, M. G. Duda, L. D. Fowler, S.-H. Park, and T. D. Ringler, 2012: A multiscale nonhydrostatic atmospheric model using centroidal Voronoi tessellations and C-grid staggering. *Monthly Weather Review*, **140** (9), 3090–3105, doi:10.1175/MWR-D-11-00215.1.
- St-Cyr, A., C. Jablonowski, J. M. Dennis, H. M. Tufo, and S. J. Thomas, 2008: A comparison of two shallow-water models with nonconforming adaptive grids. *Monthly Weather Review*, **136** (6), 1898–1922, doi:10.1175/2007MWR2108.1.
- Takahashi, Y. O., K. Hamilton, and W. Ohfuchi, 2006: Explicit global simulation of the mesoscale spectrum of atmospheric motions. *Geophysical Research Letters*, **33**, L12812, doi:10.1029/2006GL026429.
- Taylor, M., J. Tribbia, and M. Iskandarani, 1997: The spectral element method for the shallow water equations on the sphere. *J. Comput. Phys.*, **130**, 92–108.

- Taylor, M. A., 2011: Conservation of mass and energy for the moist atmospheric primitive equations on unstructured grids. *Numerical Techniques for Global Atmospheric Models*, P. H. Lauritzen, C. Jablonowski, M. A. Taylor, and R. D. Nair, Eds., Springer, Lecture Notes in Computational Science and Engineering, Vol. 80, 357–380.
- Taylor, M. A., J. Edwards, S. Thomas, and R. D. Nair, 2007: A mass and energy conserving spectral element atmospheric dynamical core on the cubed-sphere grid. *Journal of Physics: Conference Series*, **78**, 012074.
- Taylor, M. A. and A. Fournier, 2010: A compatible and conservative spectral element method on unstructured grids. *Journal of Computational Physics*, **229** (17), 5879–5895.
- Wheeler, M. and G. N. Kiladis, 1999: Convectively coupled equatorial waves: Analysis of clouds and temperature in the wavenumber–frequency domain. *Journal of the Atmospheric Sciences*, **56** (3), 374–399.
- Williamson, D. L., 2008a: Convergence of aqua-planet simulations with increasing resolution in the Community Atmospheric Model, Version3. *Tellus*, **60A**, 848–862.
- Williamson, D. L., 2008b: Equivalent finite volume and Eulerian spectral transform horizontal resolutions established from aqua-planet simulations. *Tellus*, **60A**, 839–847.
- Williamson, D. L., 2013: The effect of time steps and time-scales on parametrization suites. *Quarterly Journal of the Royal Meteorological Society*, **139** (671), 548–560, doi:10.1002/qj.1992.
- Williamson, D. L., J. B. Drake, J. J. Hack, R. Jakob, and P. N. Swarztrauber, 1992: A standard test set for numerical approximations to the shallow water equations in spherical geometry. *J. Comput. Phys.*, **102**, 211–224.
- Zarzycki, C. M., C. Jablonowski, and M. A. Taylor, 2013: Using variable resolution meshes to

model tropical cyclones in the Community Atmosphere Model. *Monthly Weather Review*, doi:10.1175/MWR-D-13-00179.1, in press.

Zhang, G. J. and N. A. McFarlane, 1995: Sensitivity of climate simulations to the parameterization of cumulus convection in the Canadian Climate Centre General Circulation Model. *Atmos.–Ocean*, **33**, 407–446.

List of Tables

- 1 CAM-SE resolutions of interest to this study. Grid spacing Δx (in kilometers and degrees) correspond to the grid spacing at the center of a cubed-sphere (CS) face. Dynamics time steps (dt_{dyn}) are globally constrained by the finest grid scale in an individual variable resolution model simulation, while the 4th-order diffusion coefficient $K_4(\Delta x)$ (hyperviscosity) is allowed to vary among individual elements. 39
- 2 Time-averaged statistics for CAM4 simulations in the equatorial band. Areas used for averaging are shown in Fig. 3. ‘Var-res’ is the component of variable-resolution simulation that corresponds to the specified grid spacing. See text for explanation of acronyms. 40
- 3 Same as Table 3 but for CAM5 simulations. 41

TABLE 1. CAM-SE resolutions of interest to this study. Grid spacing Δx (in kilometers and degrees) correspond to the grid spacing at the center of a cubed-sphere (CS) face. Dynamics time steps (dt_{dyn}) are globally constrained by the finest grid scale in an individual variable resolution model simulation, while the 4th-order diffusion coefficient $K_4(\Delta x)$ (hyperviscosity) is allowed to vary among individual elements.

Setup	CS res.	Δx ($^{\circ}$)	Δx (km)	Cells (#)	dt_{dyn} (s)	K_4 ($\text{m}^4 \text{s}^{-1}$)
fine	n_e120	0.25°	28	86,400	50	1.00E+16
coarse	n_e15	2°	222	13,500	600	1.00E+13
var-res	n_e15x8	varies	varies	10,609	50	varies

TABLE 2. Time-averaged statistics for CAM4 simulations in the equatorial band. Areas used for averaging are shown in Fig. 3. ‘Var-res’ is the component of variable-resolution simulation that corresponds to the specified grid spacing. See text for explanation of acronyms.

Variable	Units	Coarse 2°	Var-res 2°	Fine 0.25°	Var-res 0.25°
PRECC	mm d ⁻¹	2.18	2.25	1.23	1.14
PRECL	mm d ⁻¹	1.56	1.62	3.04	2.78
PRECT	mm d ⁻¹	3.75	3.87	4.27	3.91
C/L ratio		1.40	1.39	0.40	0.41
CLDTOT	frac	0.56	0.56	0.36	0.39
TPW	kg m ⁻²	33.4	33.5	32.1	31.5

TABLE 3. Same as Table 3 but for CAM5 simulations.

Variable	Units	Coarse 2°	Var-res 2°	Fine 0.25°	Var-res 0.25°
PRECC	mm d ⁻¹	3.66	3.59	2.25	2.68
PRECL	mm d ⁻¹	0.49	0.48	1.85	1.68
PRECT	mm d ⁻¹	4.15	4.08	4.10	4.36
C/L ratio		6.60	6.63	1.16	1.51
CLDTOT	frac	0.63	0.63	0.64	0.65
TPW	kg m ⁻²	32.8	32.8	31.7	31.8

List of Figures

- 1 The default quadrilateral refinement in CUBIT will refine the highlighted cells in the (a) uniform mesh, resulting in the (b) 2-refined mesh. 44
- 2 The three meshes used for this study are (a) a uniform 2° resolution mesh, (not pictured) a uniform 0.25° resolution mesh, and (b) a variable resolution mesh that ranges from $2^\circ \rightarrow 0.25^\circ$. Note that each element shown in the above plots contains additional 3×3 collocation points. 45
- 3 For Tables 2 and 3 and Figs. 4 and 8, the “fine” region statistics in var-res simulations come from the red area while the “coarse” region statistics come from the blue area. The edges of the transition region are outlined by the two black boxes. 46
- 4 Zonal mean total cloud fraction and total precipitation rate using CAM4 physics. (a) CLDTOT: Comparing the uniform 2° and 0.25° meshes with the variable resolution (VR). (b) Separating the fine region and the coarse region of the variable resolution mesh near the equator. (c) and (d) are the same except for the total precipitation rate (PRECT). 47
- 5 CAM4 contour plot of total cloud fraction (in percent) for (a) coarse (2°) (b) var-res (VR), and (c) fine (0.25°) simulations. The grey boxes denote the different mesh regions: inside the innermost box is the fine region, outside the outermost box is the coarse region, and between the boxes is the transition region. The difference between the var-res and coarse simulation is plotted in (d) and the var-res and fine simulation in (e). 48
- 6 Same as Figure 5 except for total precipitation rate (mm day^{-1}). 49
- 7 Zonal anomalies of (a) vertically integrated moist heating and (b) 200 hPa divergence (color contours) for var-res grid with CAM4 physics. In (b) the 200 hPa eddy streamfunction is contoured by $10^6 \text{ m}^2 \text{ s}^{-1}$. Negative contours are dashed. 50

8	Same as Fig. 4 except with CAM5 physics.	51
9	Same as Figure 5 except with CAM5 physics.	52
10	Same as Figure 6 except with CAM5 physics.	53
11	Same as Figure 7 but with CAM5 physics.	54
12	Wavenumber-frequency diagrams of outgoing longwave radiation averaged between 10° N/S. Unnormalized anti-symmetric (a-c) and symmetric (d-f) components of the power spectra are shown for the coarse (a and d), var-res (b and e), and fine (c and f) simulations. Dispersion curves for theoretical equatorial modes are overlaid as in Wheeler and Kiladis (1999). Inertio-gravity (IG), equatorial Rossby (ER), equatorial inertio-gravity (EIR), and Kelvin waves are marked.	55
13	Hovmöller diagram of one-year of outgoing longwave radiation (W m^{-2}) for each of the three grid types averaged between 10° N/S. A band-pass filter of wavenumbers 1 to 14 and periods between 2.5 and 20 days is contoured in black.	56
14	Precipitation histogram representing fraction of instances where 6-hourly instantaneous precipitation rates were in specific intensity bins for CAM5 simulations. Statistics are averaged between 10° N/S (logarithmic scale). Variable-resolution simulation is broken into component resolutions using the areas depicted in Figure 3. Bin sizes are 1 mm day^{-1} in the left panel and 10 mm day^{-1} on the right.	57
15	Zonal mean total cloud fraction and total precipitation using CAM5 physics package with modal (MAM) aerosol package and bulk (BAM) aerosols. All simulations use the var-res grid. (a) CLDTOT: Comparing the two aerosol packages in the var-res grid. (b) Separating the fine region and the coarse region of the variable resolution mesh near the equator. (c) and (d) are the same except for total precipitation (PRECT).	58

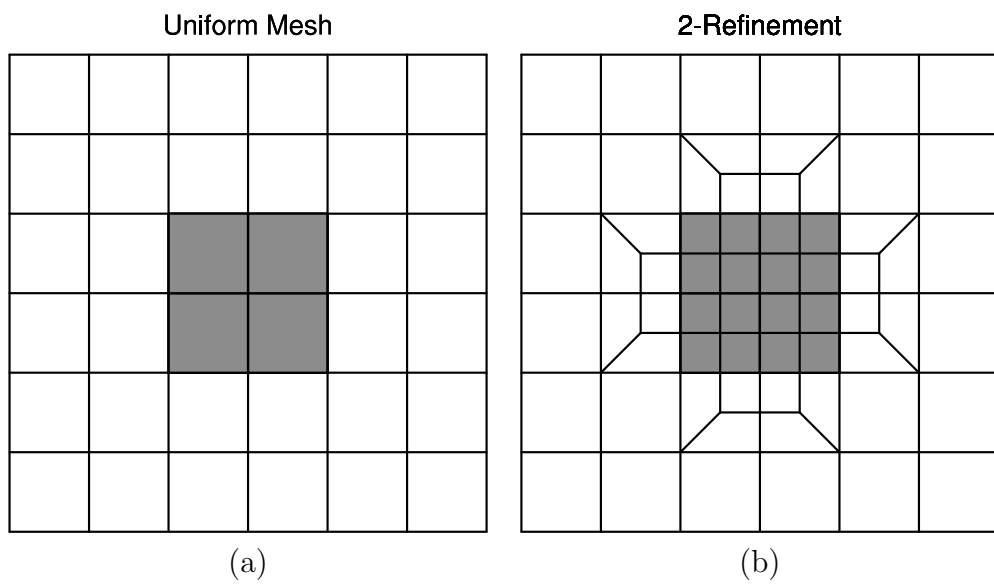


FIG. 1. The default quadrilateral refinement in CUBIT will refine the highlighted cells in the (a) uniform mesh, resulting in the (b) 2-refined mesh.

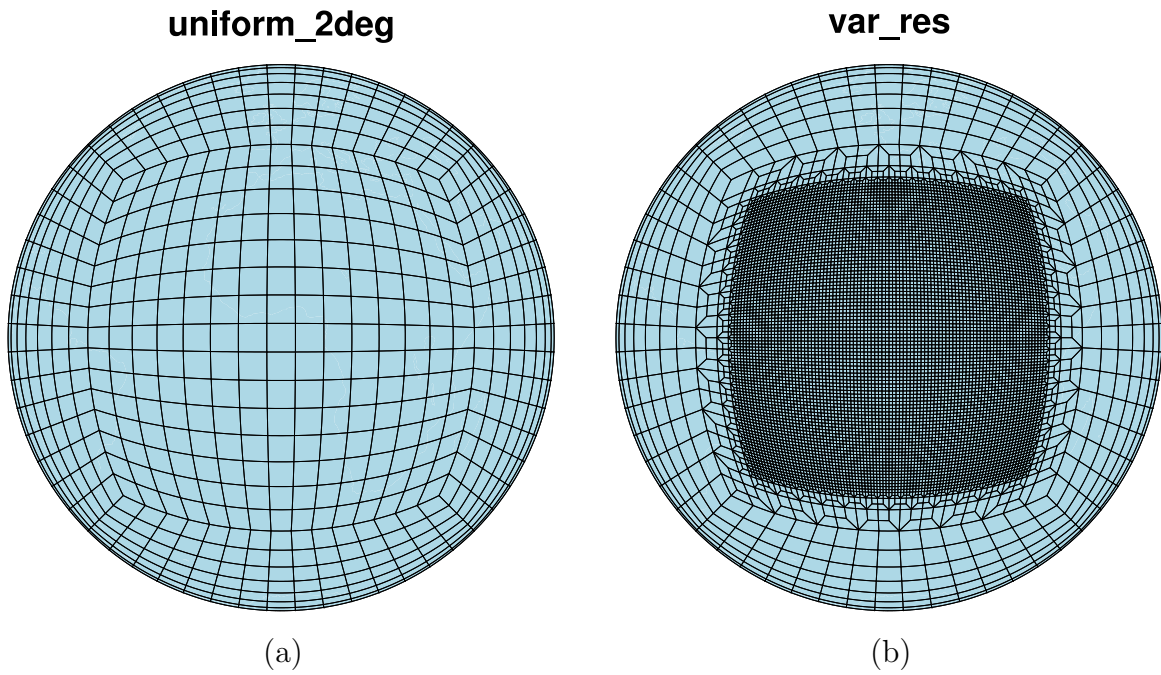


FIG. 2. The three meshes used for this study are (a) a uniform 2° resolution mesh, (not pictured) a uniform 0.25° resolution mesh, and (b) a variable resolution mesh that ranges from $2^\circ \rightarrow 0.25^\circ$. Note that each element shown in the above plots contains additional 3×3 collocation points.

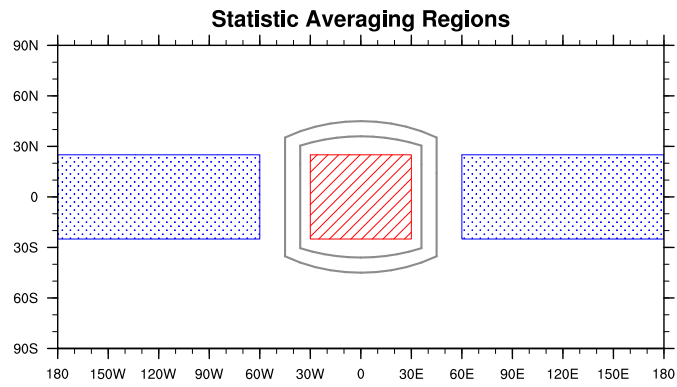


FIG. 3. For Tables 2 and 3 and Figs. 4 and 8, the “fine” region statistics in var-res simulations come from the red area while the “coarse” region statistics come from the blue area. The edges of the transition region are outlined by the two black boxes.

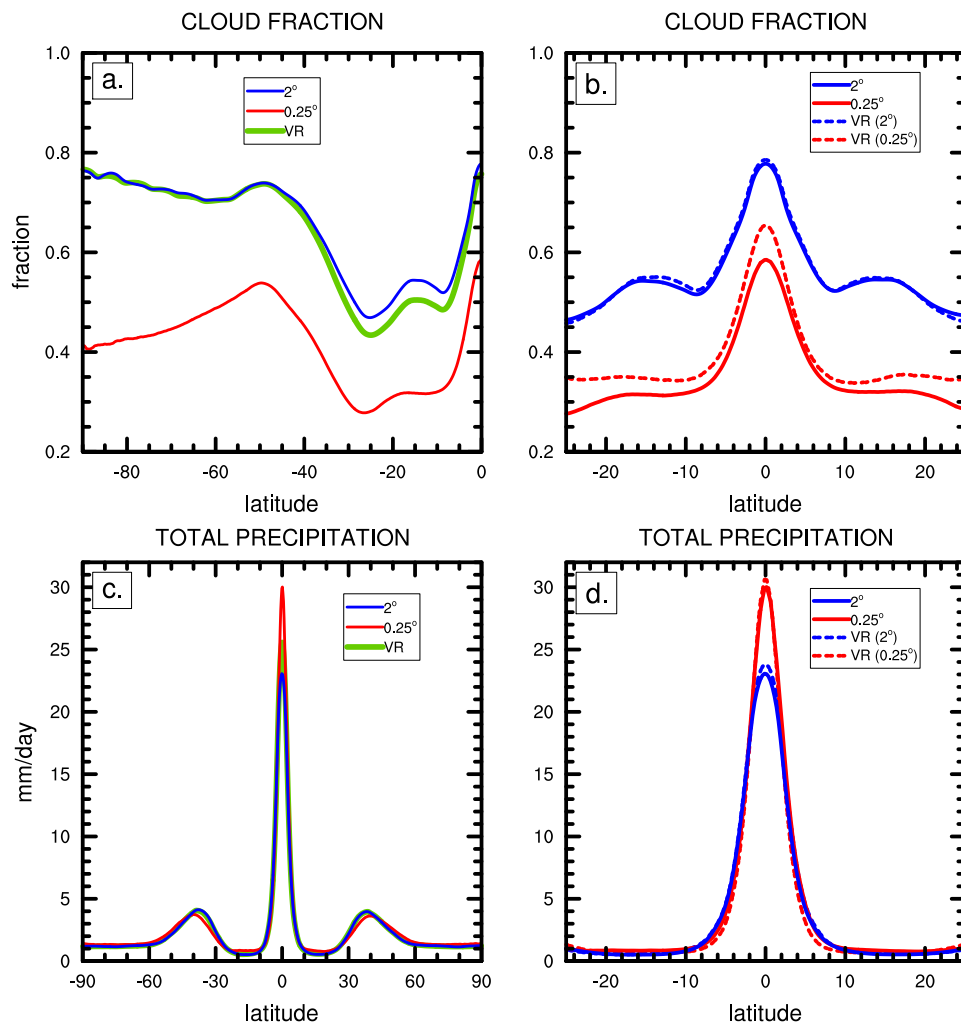


FIG. 4. Zonal mean total cloud fraction and total precipitation rate using CAM4 physics. (a) CLDTOT: Comparing the uniform 2° and 0.25° meshes with the variable resolution (VR). (b) Separating the fine region and the coarse region of the variable resolution mesh near the equator. (c) and (d) are the same except for the total precipitation rate (PRECT).

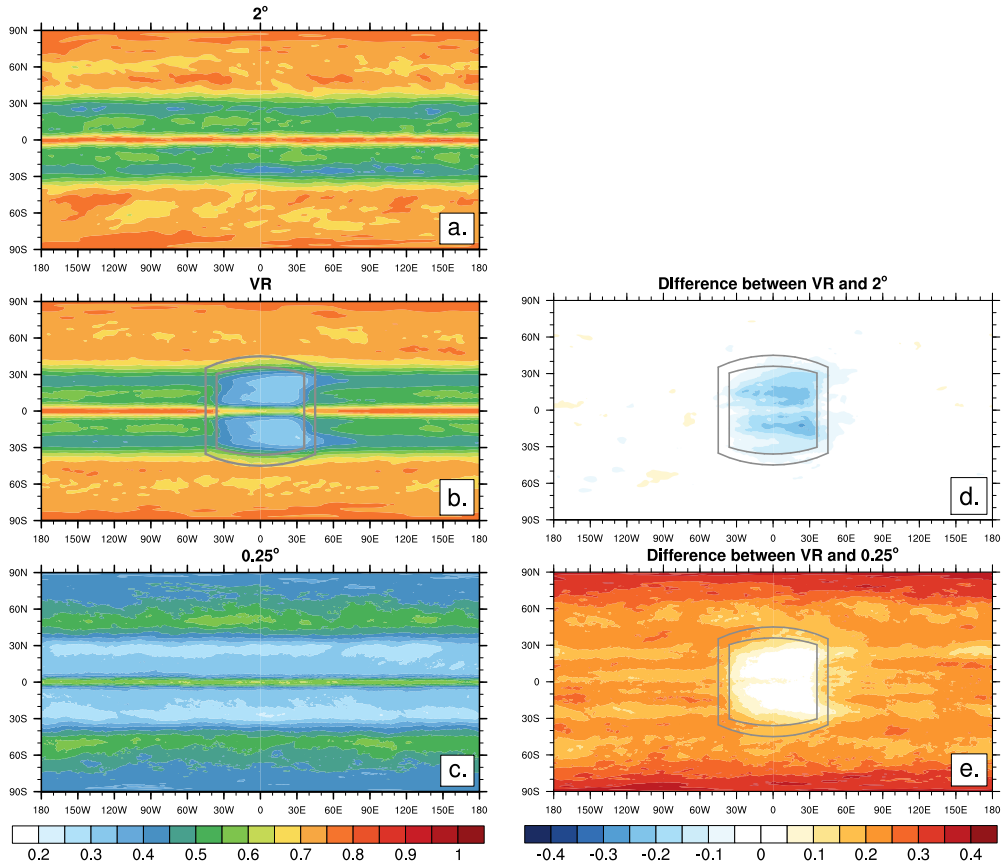


FIG. 5. CAM4 contour plot of total cloud fraction (in percent) for (a) coarse (2°) (b) var-res (VR), and (c) fine (0.25°) simulations. The grey boxes denote the different mesh regions: inside the innermost box is the fine region, outside the outermost box is the coarse region, and between the boxes is the transition region. The difference between the var-res and coarse simulation is plotted in (d) and the var-res and fine simulation in (e).

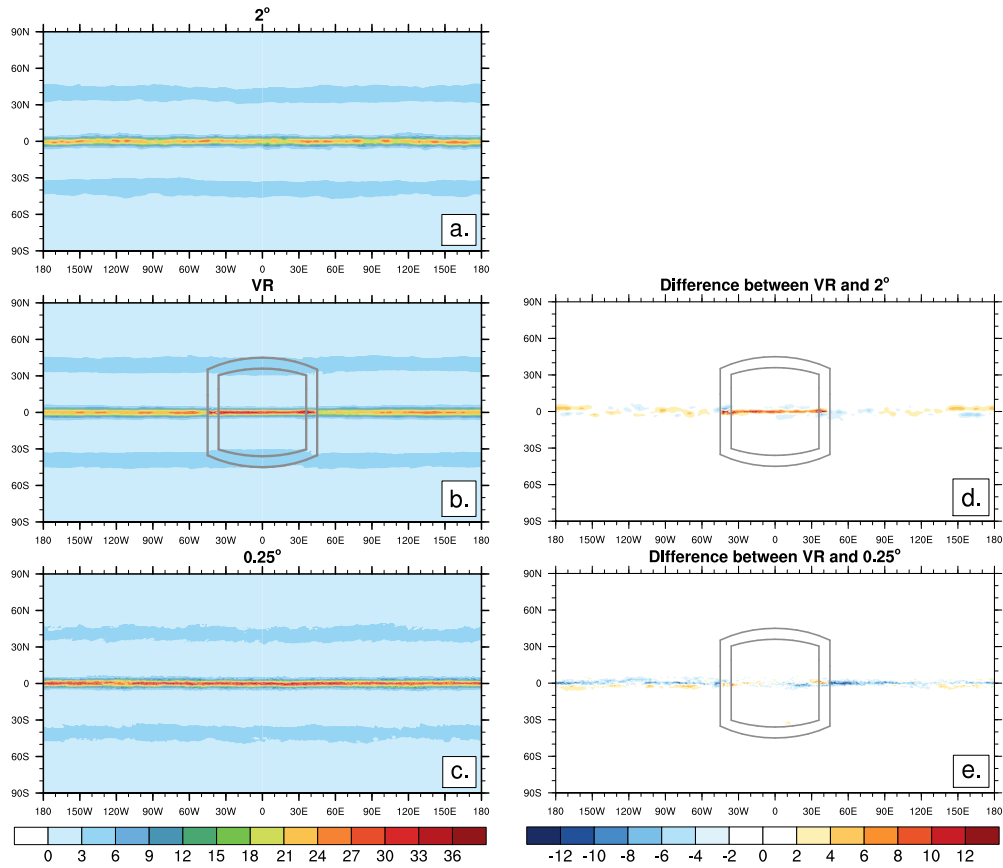


FIG. 6. Same as Figure 5 except for total precipitation rate (mm day⁻¹).

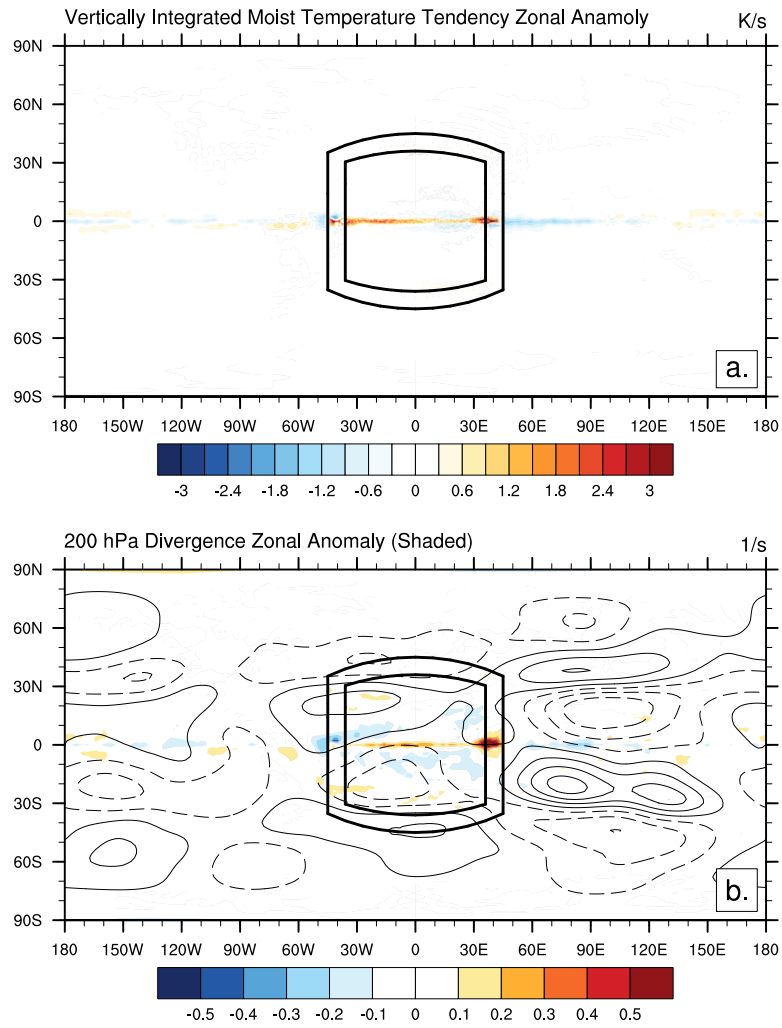


FIG. 7. Zonal anomalies of (a) vertically integrated moist heating and (b) 200 hPa divergence (color contours) for var-res grid with CAM4 physics. In (b) the 200 hPa eddy streamfunction is contoured by $10^6 \text{ m}^2 \text{ s}^{-1}$. Negative contours are dashed.

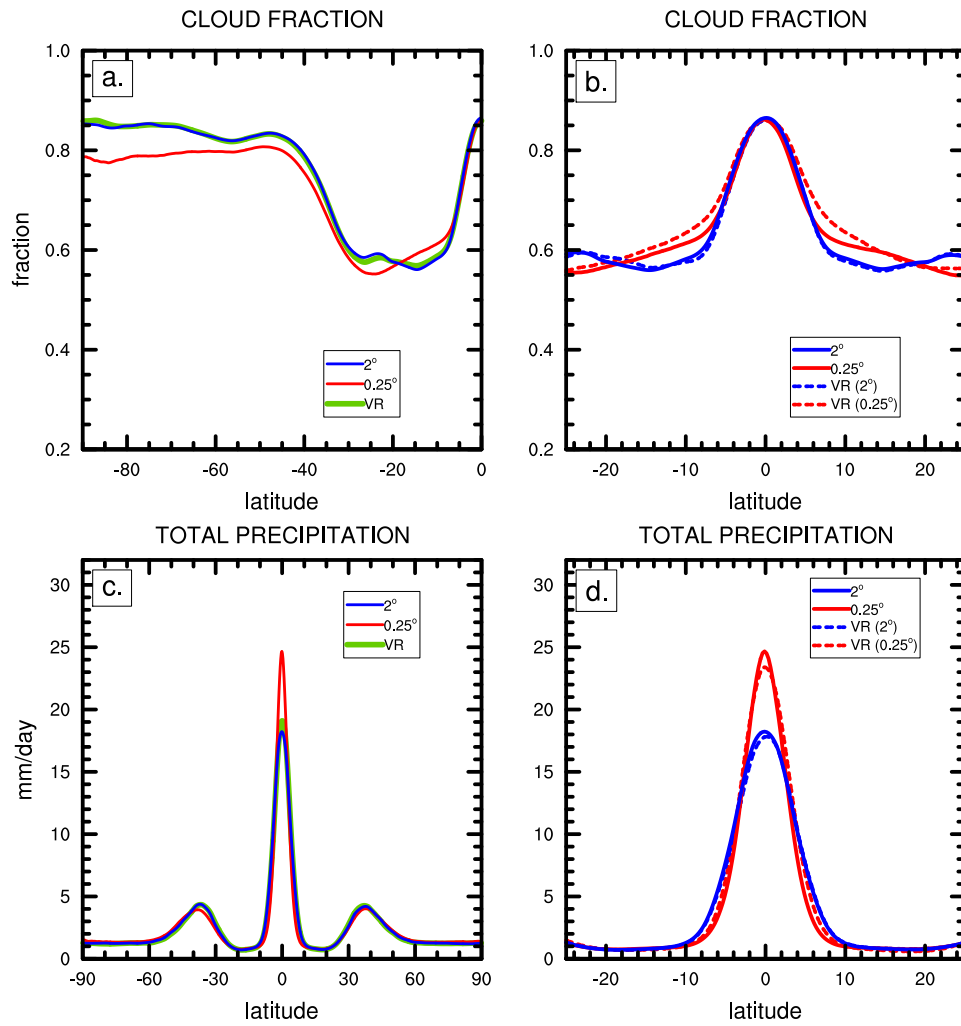


FIG. 8. Same as Fig. 4 except with CAM5 physics.

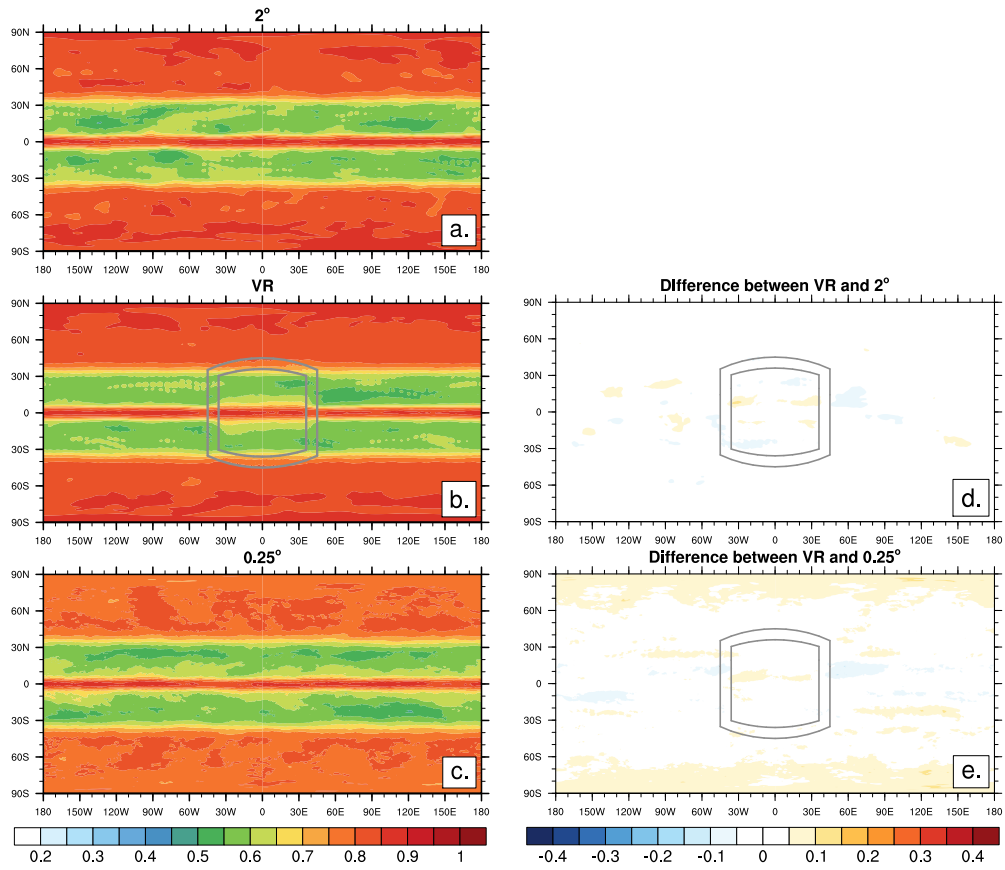


FIG. 9. Same as Figure 5 except with CAM5 physics.

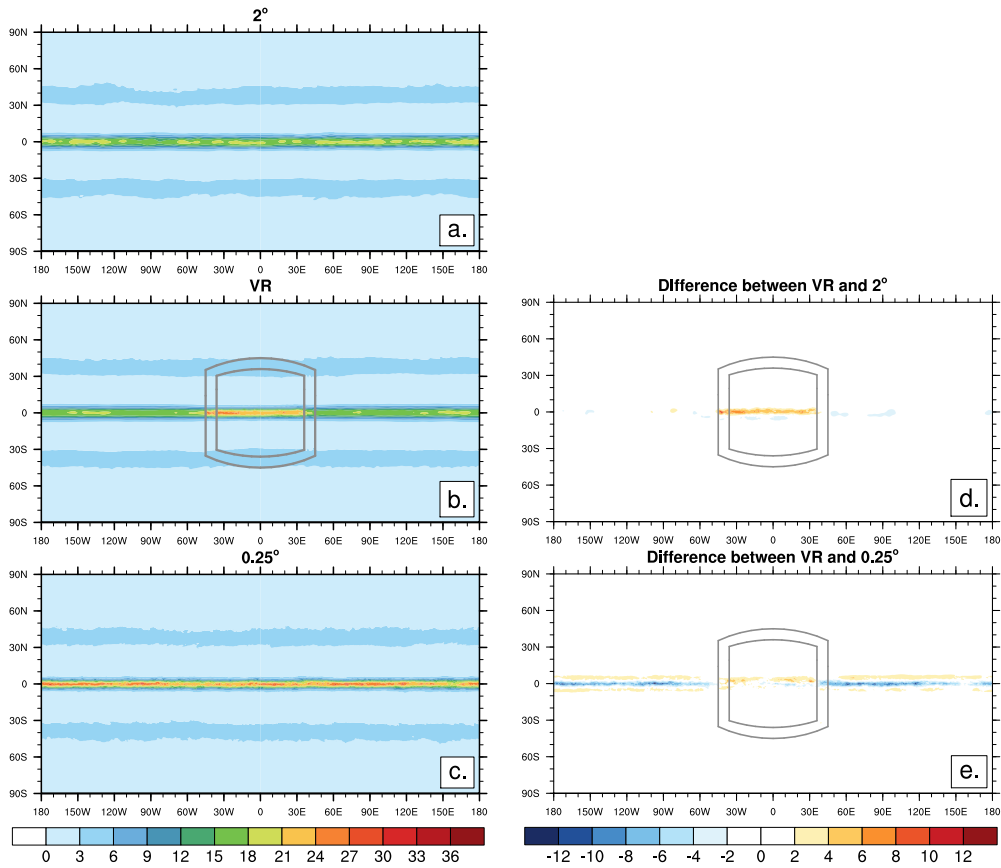


FIG. 10. Same as Figure 6 except with CAM5 physics.

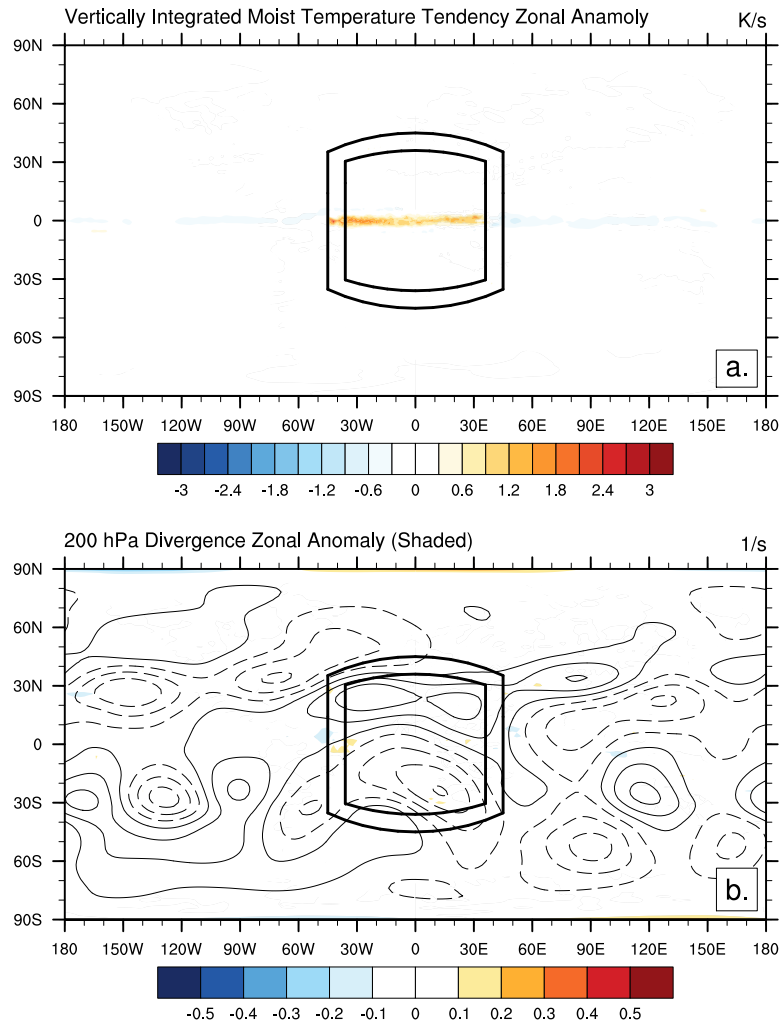


FIG. 11. Same as Figure 7 but with CAM5 physics.

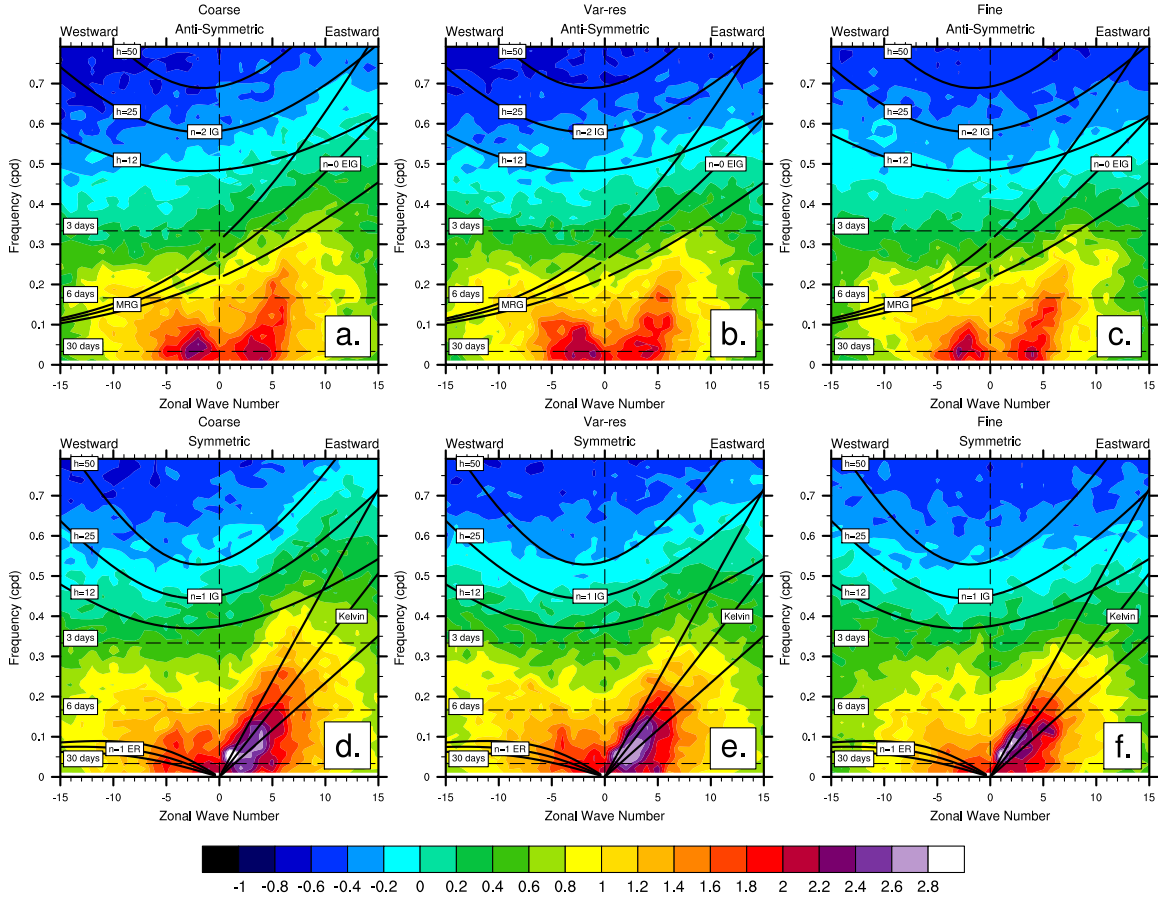


FIG. 12. Wavenumber-frequency diagrams of outgoing longwave radiation averaged between 10° N/S. Unnormalized anti-symmetric (a-c) and symmetric (d-f) components of the power spectra are shown for the coarse (a and d), var-res (b and e), and fine (c and f) simulations. Dispersion curves for theoretical equatorial modes are overlaid as in Wheeler and Kiladis (1999). Inertio-gravity (IG), equatorial Rossby (ER), equatorial inertio-gravity (EIR), and Kelvin waves are marked.

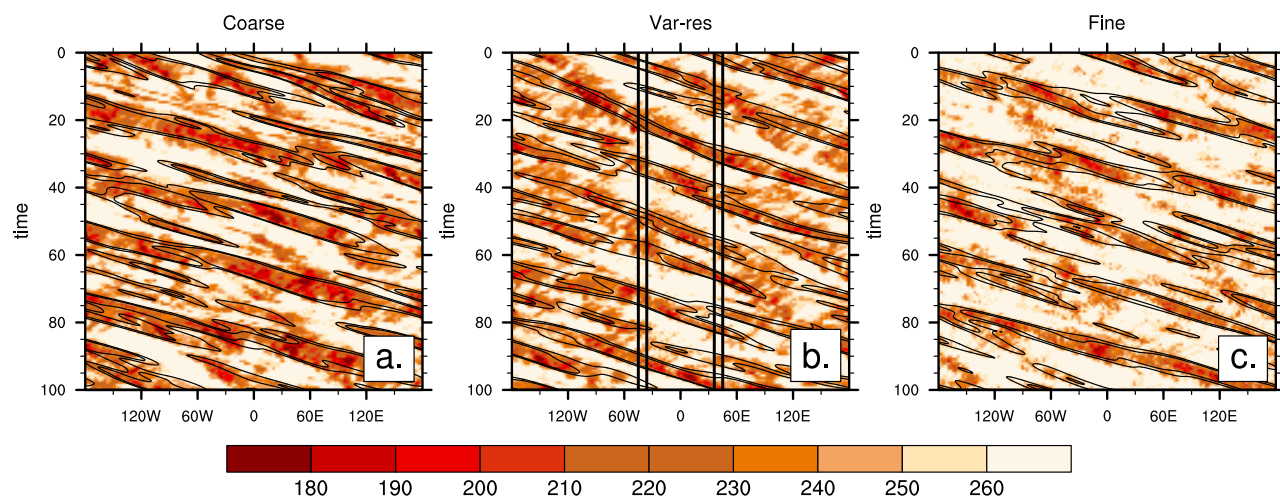


FIG. 13. Hovmöller diagram of one-year of outgoing longwave radiation (W m^{-2}) for each of the three grid types averaged between 10° N/S . A band-pass filter of wavenumbers 1 to 14 and periods between 2.5 and 20 days is contoured in black.

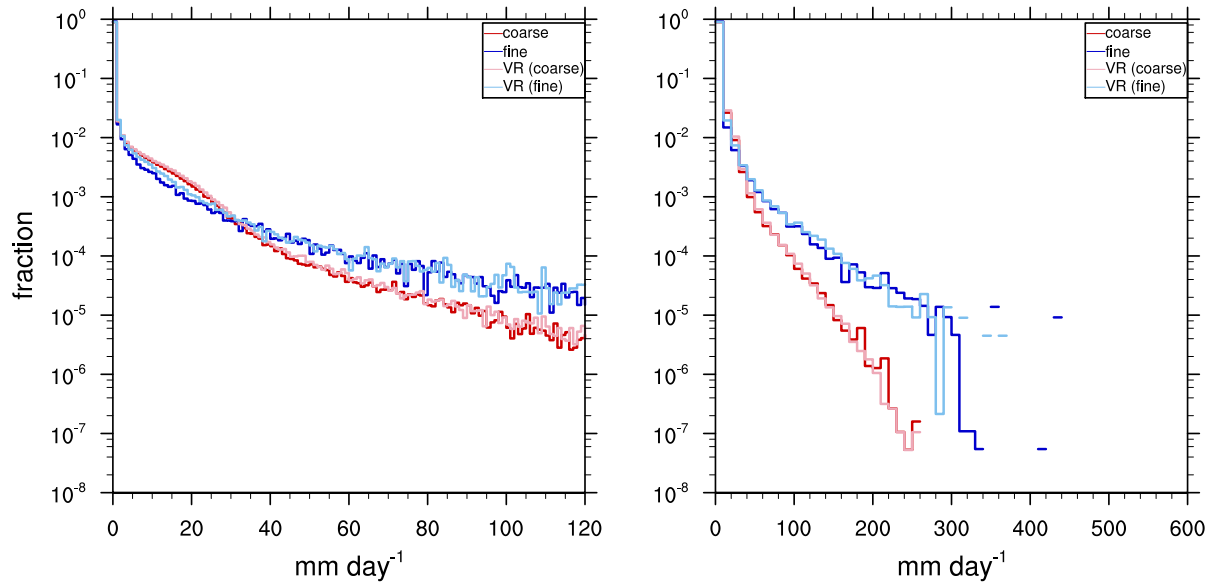


FIG. 14. Precipitation histogram representing fraction of instances where 6-hourly instantaneous precipitation rates were in specific intensity bins for CAM5 simulations. Statistics are averaged between 10° N/S (logarithmic scale). Variable-resolution simulation is broken into component resolutions using the areas depicted in Figure 3. Bin sizes are 1 mm day^{-1} in the left panel and 10 mm day^{-1} on the right.

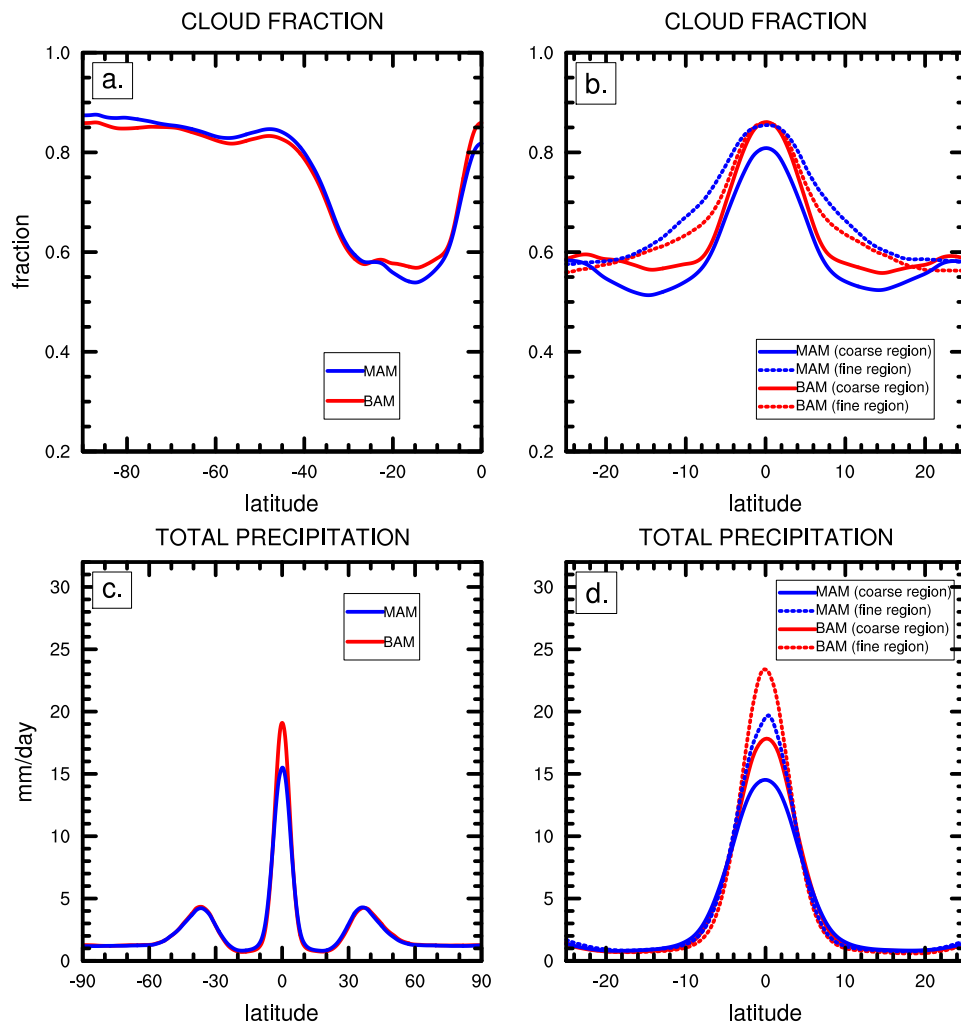


FIG. 15. Zonal mean total cloud fraction and total precipitation using CAM5 physics package with modal (MAM) aerosol package and bulk (BAM) aerosols. All simulations use the var-res grid. (a) CLDTOT: Comparing the two aerosol packages in the var-res grid. (b) Separating the fine region and the coarse region of the variable resolution mesh near the equator. (c) and (d) are the same except for total precipitation (PRECT).